

1 **Cyanobacterial diversity and related sedimentary facies as a function of water flow**
2 **conditions: Example from the Monasterio de Piedra Natural Park (Spain)**

3

4 Esther Berrendero^{1,2}, Concha Arenas^{3*}, Pilar Mateo¹, Brian Jones⁴

5 ¹*Department of Biology, Science Faculty, Autónoma University of Madrid, 28049*

6 *Madrid, Spain*

7 ²*Department of Botany, Faculty of Science, University of South Bohemia, 370 05 České*

8 *Budějovice, Czech Republic*

9 ³*Division of Stratigraphy, Department of Earth Sciences, University of Zaragoza. 50009*

10 *Zaragoza, Spain*

11 ⁴*Department of Earth and Atmospheric Sciences, University of Alberta. Edmonton,*

12 *Alberta T6G 2E3, Canada*

13

14 *Corresponding author. E-mail address: *carenas@unizar.es*.

15

16 **ABSTRACT**

17 The River Piedra in the Monasterio de Piedra Natural Park (NE Spain) is a modern tufa-

18 depositing river that encompasses various depositional environments that are

19 inhabited by different cyanobacterial populations. Molecular (16S rDNA) and

20 morphological analyses of the cyanobacteria from different facies showed that

21 *Phormidium incrustatum* dominates in the fast-flowing water areas where the mean

22 depositional rate is 1.6 cm/year. Stromatolites in these areas are formed of palisades

23 of hollow calcite tubes (inner diameter of 6.0-7.5 μm , walls 2-12 μm thick) that formed

24 through calcite encrustation around the filaments followed by decay of the trichomes.

25 In contrast, in slow-flowing water areas with lower depositional rates (mean
26 depositional rate of 0.3 cm/yr), *Phormidium aerugineo-caeruleum* is the dominant
27 species. In these areas, randomly oriented calcite tubes (inner diameter of 5-6 μm ,
28 walls 3-8 μm thick) formed by calcite encrustation, are found in thin and uneven
29 laminae and as scattered tubes in the loose lime mud and sand-sized carbonate
30 sediment. Although this species did not build laminated deposits, it gave cohesiveness
31 to the loose sediment. In the stepped and low waterfalls, with intermediate deposition
32 rates (mean depositional rate of 0.9 cm/yr), both species of *Phormidium* are found in
33 association with spongy moss and algal boundstones, which is consistent with the
34 variable flow conditions in this setting.

35 The calcite encrustations on the cyanobacteria from different environments
36 exhibit irregular patterns that may be linked to changes in the calcite saturation index.
37 The physicochemical conditions associated with extracellular polymeric substances
38 may be more significant to CaCO_3 precipitation in microbial mats in slow-flowing water
39 conditions than in fast-flowing water conditions. These results show that flow
40 conditions may influence the distribution of different cyanobacteria that, in turn, leads
41 to the development of different sedimentary facies and structures in fluvial carbonate
42 systems.

43

44 **Key words:** Cyanobacterial diversity, fluvial tufa facies, varied depositional settings,
45 recent carbonate sedimentation

46

47

48 **1. Introduction**

49 The roles that climatic, hydrological variables, and microbial communities play in
50 the development of the sedimentary record in modern fluvial carbonate systems have
51 been the focus of many studies (e.g., Janssen et al., 1999; Shiraishi et al., 2008; Pedley
52 et al., 2009; Gradziński, 2010; Vázquez-Urbez et al., 2010; Manzo et al., 2012). In fluvial
53 carbonate environments (Arp et al., 2001; Pentecost, 2005; Santos et al., 2010; Beraldi-
54 Campesi et al., 2012) there is typically a high diversity of bacteria that commonly
55 mediate the development of various organosedimentary structures, including
56 stromatolites and oncolites.

57 Filamentous and coccoid cyanobacteria, which are photosynthetic prokaryotes
58 that can live in a wide range of environments, play a major role in the growth and
59 development of stromatolites, as recognized in both modern (Reid et al., 2000; Arp et
60 al., 2001; Santos et al., 2010; Shiraishi et al., 2010) and fossil examples (Awramik, 1991;
61 Golubić et al., 2000; Riding, 2000). It has been suggested that cyanobacteria have
62 become the most successful mat-building organisms, possibly because they can
63 photosynthesize even under extremely low light conditions (Schopf, 2012). Their role
64 in microbialite formation, however, is not fully understood and the relationship
65 between cyanobacterial communities, environmental conditions, and the resulting
66 structures is poorly known.

67 Actively forming tufa found in various fluvial environments in the River Piedra (Fig.
68 1) has been the focus of a thirteen-year study of modern sedimentation. The
69 dominant facies are (1) dense laminated tufa, (2) loose lime mud and sand that
70 commonly lack laminations, and (3) spongy, moss- and alga-bearing tufa that is either
71 coarsely laminated or non-laminated (Arenas et al., 2014). Modern fluvial tufa systems

72 in NE Spain, including those in the River Piedra, are characterized by a high diversity of
73 bacteria with cyanobacteria being dominant (approximately 43%; Beraldi-Campesi et
74 al., 2012). In the River Piedra, cyanobacterial mats are found in variably flow conditions
75 that include fast- and slow-moving water. The different attributes of the structures
76 found in these contrasting flow conditions are, however, unknown. Thus, the main aim
77 of this paper is to compare the cyanobacterial diversity and related sedimentary facies
78 that develop in these contrasting flow conditions. This is achieved by examining the
79 (1) dominant cyanobacterial populations in each of the main depositional
80 environments found in the river, (2) cyanobacterial structures that developed on
81 artificial substrates over a period of 13 years, and (3) calcification of the cyanobacteria.
82 Integration of this information provides an assessment of the relationships between
83 the environmental parameters and the cyanobacterial structures that are evident in
84 the tufa. As far as we are aware, this is the first study in which morphological and
85 phylogenetic (16S rDNA) analyses have been used to determine the relationship
86 between different depositional structures and calcification style of the dominant
87 cyanobacterial constituents, relative to the physical and chemical attributes of the
88 fluvial system. As such, the results have important implications for similar depositional
89 systems throughout the world.

90

91 **2. Geological setting, hydrology and climate**

92 This study, conducted in the Monasterio de Piedra Natural Park (NE Spain),
93 focused on the lower reaches of the northward flowing River Piedra, which is a
94 tributary of the River Ebro (Fig. 1A). From its headwaters to its mouth in the La

95 Tranquera Reservoir, the river flows across Mesozoic and Cenozoic carbonates and
96 siliciclastics (Fig. 1A), and Quaternary tufa deposits.

97 The River Piedra is fed mainly by an aquifer that is located in Lower Jurassic and
98 Upper Cretaceous limestones and dolostones. The most important natural springs,
99 with a flow of $\sim 1.4 \text{ m}^3/\text{s}$, are located near the village of Cimballa (Fig. 1A). The mean
100 river discharge is $\sim 1.06 \text{ m}^3/\text{s}$ (measured downstream from the Natural Park between
101 October 1999 and September 2012; data from *Confederación Hidrográfica del Ebro*,
102 <https://195.55.247.237/saihebro>). Water in the River Piedra is of the $\text{HCO}_3\text{-(SO}_4\text{)-Ca}$
103 type. Downstream of the springs at Cimballa, the water has a conductivity of 503–734
104 $\mu\text{S/cm}$, alkalinity of 238–350 mg/L, Ca concentrations of 75–112 mg/L, SO_4
105 concentrations of 54–157 mg/L, and pH of 7.7–8.5 (data from analyses from 1999 to
106 2012; Arenas et al., 2014).

107 The climate of the area is continental Mediterranean with strong seasonal
108 contrasts in temperature and precipitation. Between October 1999 and September
109 2012, mean annual air temperature was 13.1°C . Air temperature was highest in July
110 and August (monthly mean values of $21.7\text{--}25.0^\circ\text{C}$), and lowest between December and
111 February (monthly mean values of $2.4\text{--}7.0^\circ\text{C}$). Water temperature ranged from 16.5 to
112 17.7°C in July and August to 9 to 10°C in December and January. During the same
113 period, mean annual rainfall was 397.4 mm (based on data from the La Tranquera and
114 Milmarcos meteorological stations), with maxima in April, May, and October (air
115 temperature and precipitation data from *Agencia Estatal de Meteorología*).

116 Close to the Monasterio de Piedra Natural Park, the gradient of the River Piedra
117 becomes steeper than in upstream reaches. In the park, caves have formed behind the
118 Caprichosa and Cola de Caballo waterfalls that have vertical drops of 15 and 35 m,

119 respectively (Fig. 1B). Other fluvial features are (1) rapids, (2) slow-flowing water areas
120 that have formed upstream of small waterfalls, and (3) small waterfalls along the river
121 (in places damming water upstream) and several stepped waterfalls (5 to 10 m high)
122 that have developed on the riversides.

123 **3. Terminology**

124 Given the diversity of depositional settings in the fluvial system, the term
125 “environment” herein refers to areas that are characterized by distinct physical and
126 biological attributes (e.g., physical flow characteristics, morphological features of the
127 river bed, biota). Facies refer to different types of sediments that are defined by their
128 textural components and their sedimentary structures.

129 The term “microbialite” is used *sensu* Burne and Moore (1987, pp. 241-242) to
130 designate “...organosedimentary deposits that have accreted as a result of a benthic
131 microbial community trapping and binding detrital sediment and/or forming the locus
132 of mineral precipitation”. Laminated microbialites that grow on the sediment surface
133 are termed stromatolites (cf., Riding, 1991).

134 A biofilm consists of a microbial community that is embedded in extracellular
135 polymeric substances (EPS) (Rosenberg, 1989; Neu, 1996; Decho, 2010). Typically, the
136 EPS is a hydrogel that allows microbes to attach themselves to substrates while
137 buffering them from the immediate extracellular environment (Decho, 2010).

138 Krumbein et al. (2003, pp. 13) considered that “microbial mats are intimately
139 interwoven microbial communities including laminated, concentric and network like
140 growth patterns, which by their upward directed growth, physical and chemical
141 gradients, barriers and sticky EPS products trap and embed mineral grains, produce
142 new minerals and, ultimately, laminated and spherulitic sedimentary rocks and

143 structures". Microbial mats involve stratification of the microbial populations into
144 several layers. They may therefore be considered as complex biofilms (Stolz, 2000). Arp
145 et al. (2001, 2010) considered that tufa stromatolites result from calcification of
146 cyanobacterial-dominated biofilms. Herein, the term "microbial/cyanobacterial mat"
147 is used in a general sense and refers to microbial/cyanobacterial populations that coat
148 the substrate, independent of the complexity of their internal structure.

149 **4. Materials and methods**

150 *4.1. Sample collection and related parameters*

151 Samples for cyanobacterial analysis were collected in September 2010 from eight
152 sites in the Monasterio de Piedra Natural Park (Fig. 1B). These sites included three
153 different fluvial environments (Figs. 2A, 3A, 4A) with that include facies A, B, and C
154 (Table 1). At each site, samples were taken from the uppermost surface of the
155 deposits. Part of each sample was fixed in 4% formaldehyde for microscopic
156 observation, and two other parts were kept at low temperature during transport to
157 the laboratory before being frozen prior to genetic analyses.

158 Data for each sampled site came from a comprehensive study of the River Piedra
159 that took place between 1999 and 2012. Water velocity and depth were measured
160 every three months (at the end of each season), and various hydrochemical
161 parameters were measured every six months (end of December or beginning of
162 January, and end of June), following the procedures outlined in Arenas et al. (2014).
163 Deposition rates were determined from the sediment that accumulated on the
164 artificial substrates (limestone tablets, 25 x 16 x 2 cm) that had been placed in the river
165 between 1999 and 2012. Sediment thickness on the tablets was measured at the end
166 of March and the end of September, so that deposition rates corresponded to six-

167 month periods (April–September: warm period; October–March: cool period). Once
168 removed, the tablets were cut perpendicular to the accumulation surface, and the six-
169 month intervals were identified on the cross-sections by plotting the successive
170 thickness measurements on the corresponding raw cuts (see procedure details in
171 Vázquez-Urbez et al., 2010 and Arenas et al., 2014). These data include the six-month
172 period (April–September 2010) that is the focus of this study (Tables 1, 2).

173

174 *4.2. Laboratory analyses*

175 The structures and textures of the carbonate deposits that formed on the tablets
176 were documented by thin section and scanning electron microscope (SEM) analyses in
177 the Servicio de Apoyo a la Investigación (SAI) facilities of the University of Zaragoza
178 (Spain) and University of Alberta (Canada). Such analyses provided critical information
179 on the calcification structures, size and shape of crystals, and other components that
180 collectively control the textures of the carbonates. Samples (up to approximately 1.5 x
181 1 x 0.5 cm) were selected for SEM analyses from deposits that corresponded to
182 different six-month periods. The samples were coated with gold or carbon. Common
183 working conditions were 3-5 kV and 150-500 pA. SEM analyses were done on a JEOL
184 JSM 6400 scanning electron microscope (SEM) (JEOL Limited, Tokyo, Japan) and Carl
185 Zeiss MERLIN™ (Carl Zeiss Group, Jena, Germany).

186

187 *4.3. Morphological characterization of cyanobacteria*

188 The morphology of the cyanobacteria in the collected samples were imaged using
189 an Olympus BH2-RFCA photomicroscope equipped with phase-contrast,
190 epifluorescence and video camera systems (Leica DC Camera; Leica Microsystems).

191 Morphological identifications follow Komárek and Anagnostidis (1998, 2005) and
192 Whitton (2011). Their percentage abundance in the samples was evaluated by
193 counting the presence of each species (as cells in a filament or as equal numbers of
194 individual cells) as a percentage of all cells counted.

195

196 4.4. DNA extraction, amplification of the 16SrRNA gene, cloning and sequencing

197 Genomic DNA from field samples was extracted following a modification of a
198 technique for isolating DNA from fresh plant tissue that utilizes
199 cetyltrimethylammonium bromide (CTAB), as described by Berrendero et al. (2008).
200 The 16S rRNA gene sequences were amplified from the genomic DNA using primers pA
201 (Edwards et al., 1989) and cyanobacteria-specific B23S (Lepère et al., 2000).
202 Amplifications by polymerase chain reaction (PCR) were performed in a 25- μ l reaction
203 volume, following the method of Berrendero et al. (2008), under the conditions
204 described by Gkelis et al. (2005). PCR products were cloned into pGEM-T vectors using
205 the pGEM-T Easy Vector system (Promega), in accordance with the manufacturer's
206 recommendations, and transformed into DH5 α chemically competent *Escherichia coli*.
207 Clones were screened for inserts by PCR amplification with the aforementioned
208 primers. Correct-sized amplified products were purified using the Real Clean Spin kit
209 (Real) and sequenced with a BigDye Terminator v3.1 Cycle Sequencing Kit in the ABI
210 Prism 3730 Genetic Analyzer (Applied Biosystems), according to the manufacturer's
211 instructions. Sequences were obtained for both strands independently. Clones are
212 named after the sampling site and the number of the selected transformed colony.
213

214 *4.5. Analysis of nucleotide sequence data*

215 Nucleotide sequences obtained from DNA sequencing were compared with
216 information available from the National Center for Biotechnology Information
217 database using the Basic Local Alignment Tool (BLAST)
218 (<http://www.ncbi.nlm.nih.gov/BLAST>). Taxonomic identity was assigned to sequences
219 based upon the sequence identity matches on BLAST. Each sequence was checked for
220 identification-anomalous 16S rRNA gene sequences with the DECIPHER's Find
221 Chimeras web tool (Wright et al., 2012;
222 <http://decipher.cce.wisc.edu/FindChimeras.html>).

223 For the phylogenetic analysis, the 16S rDNA sequences of unicellular and non-
224 heterocystous cyanobacteria most closely related to the sequences obtained and
225 longer than 1000 bp were downloaded from GenBank, where available. These, our
226 own sequences, and that of an outgroup taxon were aligned by MAFFT v. 6 (Kato and
227 Standley, 2013; <http://mafft.cbrc.jp/alignment/server/>). Alignments were manually
228 corrected to remove ambiguous sites with the BioEdit program (Hall, 1999).

229 The alignment was submitted to FindModel (<http://www.hiv.lanl.gov>), which
230 determined that the general time reversible (GTR) model with a gamma distribution of
231 rate variation was the most appropriate model (Tavare, 1986). Phylogenetic trees were
232 generated using the MEGA 6.0 program (Tamura et al., 2013).

233 For maximum likelihood (ML) analysis, the GTR model was selected, assuming a
234 discrete gamma distribution with four categories of site-to-site variability of change
235 with the nearest-neighbor-interchange algorithm. Distances for the neighbor-joining
236 (NJ) tree were estimated by the algorithm of Jukes and Cantor (1989); nucleotide
237 positions containing gaps and missing data were initially retained for all such sites in

238 the analyses, and then excluded as necessary in the pairwise distance estimation
239 (pairwise deletion option). One thousand bootstrap replicates were run to evaluate the
240 relative support of branches in all analyses; bootstrap values greater than 50% were
241 indicated at the nodes of the trees.

242 **5. Depositional environments and sedimentary facies**

243 The fluvial environments in the study area (Figs. 2-4), distinguished by the riverbed
244 geometry, physical flow characteristics (e.g., water velocity, depth), and floral and
245 bacterial associations (Vázquez-Urbez et al., 2010; Arenas et al., 2014), are divided
246 into: (1) fast-flowing water areas (Fig. 2A), (2) slow-flowing water areas (Fig. 3A), (3)
247 stepped waterfalls and small waterfalls, 1 to 10 m high (Fig. 4A), (4) vertical waterfalls
248 (15 to 35 m high) with moss and other macrophytes, and (5) spray and splash areas
249 near the waterfalls. The first three environments, targeted for cyanobacterial analyses
250 (Table 1; Figs. 2-4) because they are the largest and easiest areas to access, include
251 three dominant facies (A, B, and C).

- 252 • **Facies A** (stromatolites) consists of dense laminated deposits that developed
253 from cyanobacterial mats. Deposits that formed on the tablets were well
254 laminated, with laminae up to 6 mm thick (Fig. 2C, D). Two to five laminae
255 formed over a six-month interval.

256 This facies formed in the gentle- to steep-sloped areas with fast-flowing
257 water (velocity > 90 cm/sec) that lack macrophytes (Fig. 2A). They are, however,
258 covered by well-developed microbial mats that form brown to gray, hard surfaces
259 with smooth to knobby topographies (Fig. 2B). Facies A is also found in zones of
260 strong flow associated with the stepped waterfalls and small waterfalls (Fig. 4),

261 where the corresponding microbial mats are not extensive and give rise to
262 stromatolite interbeds within the dominant macrophyte deposits that constitute
263 facies C.

264 • **Facies B** consists of lime mud, sand-sized carbonate particles, diatoms,
265 macroscopic algae, scattered oncoids and intraclasts, along with uneven
266 interbeds of stromatolites. Deposits on the tablets, characterized by poorly
267 defined or no laminations (Fig. 3D, E), consist of loose sediment that includes
268 very thin and uneven laminae consisting of cyanobacterial calcite that form thin,
269 discontinuous interbeds of stromatolites (Fig. 3D).

270 This facies developed in the slow-flowing water areas (velocity < 80 cm/s)
271 where large patches of soft, greenish to gray microbial mats lie on the sediment
272 (Fig. 3A-C).

273 • **Facies C** is formed of spongy moss and alga boundstones. The deposits on the
274 tablets are formed largely of moss and macroscopic algae (probably *Vaucheria*
275 and *Cladophora*) that are coated by calcite, and include rare, very thin and
276 discontinuous irregular cyanobacterial calcite masses, and form spongy
277 boundstones (Fig. 4C, D).

278 Facies C is dominant around the stepped waterfalls and small waterfalls
279 (Fig. 4A). This environment includes fast- and moderate- to slow-flowing water
280 areas. On the surface, the microbial mats in facies C develop as soft, greenish to
281 gray, poorly calcified patches (Fig. 4B), which are limited in extent by growth of
282 the dominant macrophytes. Centimeter-thick, dense stromatolite layers (Facies
283 A), formed in zones of stronger flow in the waterfalls, may be interbedded with
284 the spongy boundstones (Fig. 4C, D).

285 Textural analysis of the deposits on the tablets showed that they are largely
286 biological substrates (e.g., grasses, mosses, algae and bacteria) that are coated with
287 calcite. Calcite impregnation of biological substrates (e.g., cyanobacterial filaments) is
288 less common. The matrix between these components is usually a heterogeneous mass
289 of calcite crystals, diatoms and tufa fragments, along with extracellular polymeric
290 substances (EPS).

291

292 **6. Results**

293 *6.1. Cyanobacterial phylotypes and corresponding morphotypes*

294 *6.1.1. Phylogenetic assignments*

295 Analysis of the amplified and cloned environmental DNA revealed 56 good-quality
296 sequences of approximately 1250 bp (Fig. 5). Comparison with the GenBank archival
297 database indicated that most belonged to the order Oscillatoriales (Table 3) with
298 several species of *Phormidium*. One sequence showed a high percentage of similarity
299 with the 16S rDNA sequence of the unicellular cyanobacterium *Chamaesiphon*
300 *subglobosus* PCC 7430.

301 The phylogenetic tree, constructed together with 43 cyanobacterial sequences
302 from the public database Gen Bank public domain, showed that the retrieved
303 sequences belong to four distinct clusters, although most of the sequences are in
304 clusters I and III (Fig. 5). Cluster I, which is the largest, is formed of 36 sequences that
305 were found from all sampling sites (Phylotype I). In addition, three sequences from
306 various *Microcoleus* species, and several *P. autumnale* sequences from the database
307 belong to this group. Cluster II consists of two sequences obtained in this study
308 (Phylotype II) and a freshwater strain of cf. *Wilmottia* from Canterbury (New Zealand),

309 which received strong bootstrap support. Cluster III includes 16 sequences from three
310 out of the seven sampling sites (Phylotype III) together with two environmental
311 sequences of *P. aerugineo-caeruleum* from other Spanish rivers (Loza et al., 2013).
312 Phylotype IV, composed by a sequence from this study and other freshwater
313 *Chamaesiphon* sequences from the database, corresponds to a *Chamaesiphon* cluster.

314

315 6.1.2. Morphological analysis

316 The morphological identification of the tufa-forming cyanobacteria by optical
317 microscopy (from *in situ* surface samples) showed that most of them are members of
318 the Oscillatoriales group (Fig. 6, Table 4).

319 *Phormidium incrustatum* (Naegeli) Gomont ex Gomont 1892 (Fig. 6A, B) and *P.*
320 *aerugineo-caeruleum* (Gomont) Anagnostidis et Komárek 1988 (Fig. 6C) are the
321 dominant morphospecies. *P. incrustatum* is characterized by simple, cylindrical,
322 isopolar and non-branched filaments that form irregular clusters or dark blue-green
323 colonies with more or less parallel-oriented trichomes. The filaments, with a thin
324 sheath and unstricted trichomes, have cells 6-8 μm -wide, and attenuated trichome
325 tip with weakly conical terminal cell.

326 *P. aerugineo-caeruleum* (Gomont) (Fig. 6C) is characterized by a dark blue-green
327 thallus or solitary, scattered filaments. The variously curved unbranched filaments are
328 encased by non-lamellated colorless sheaths. Trichomes, which are cylindrical,
329 unstricted and not attenuated at the ends, are composed of cells 5.5-7.0 μm wide
330 and up to half as long as wide or almost isodiametric. The broadly rounded apical cells
331 lack calyptra. The cell content is granulated.

332 A third morphotype, *Phormidium* sp., is also present in the studied samples. This
333 morphotype is characterized by straight, unstricted trichomes, 3.5-4.0 μm in
334 diameter, with abruptly narrowing and commonly bent ends. Cell length is typically
335 less than cell width and the apical cells being slightly conical or almost cylindrical and
336 rounded and without calyptra (Fig. 6D, E).

337 Other non-heterocystous filamentous cyanobacteria found in small numbers (\leq
338 4%) include *Leptolyngbya truncata* (Lemmermann) Anagnostidis et Komárek 1988 (Fig.
339 6F) and *L. foveolarum* (Rabenhorst ex Gomont) Anagnostidis et Komárek 1988 (Fig. 6G,
340 H). The former has irregularly and feebly curved filaments composed of pale blue-
341 green and non-constricted trichomes that are 0.8-1.3 μm wide (Fig. 6F), whereas the
342 latter has constricted trichomes with cells 1-1.5 μm wide that are not attenuated at
343 the end and have rounded or hemispherical apical cells (Fig. 6G, H). Other species of
344 *Leptolyngbya* (Fig. 6I, J) have non-constricted and straight trichomes formed of
345 approximately isodiametric cells, 2-3 μm wide, with truncated apical cells and
346 enveloped by thin, colorless sheaths.

347 Several species of unicellular cyanobacteria are also present, including
348 *Aphanocapsa* sp., *Aphanothece* sp. and *Chamaesiphon* sp. (Fig. 6K, L). These
349 cyanobacteria were rare in all the samples studied (\leq 3%).

350 Diatoms, including *Cocconeis placentula*, *Gyrosigma obtusatum*, *Bacillaria*
351 *paxillifera*, *Amphora* sp. and *Navicula* sp. are commonly associated with the
352 cyanobacteria (Figs. 7-9).

353

354 *6.1.3. Relationships between cyanobacterial morphotypes, phylotypes, and*
355 *sedimentary facies*

356 In the stromatolites of Facies A, *P. incrustatum* is the dominant morphotype,
357 jointly with phylotype I. On the basis of the dominant morphotype found at these
358 locations and the genetic distance to *P. autumnale* (best BLAST hit), phylotype I was
359 ascribed to *P. incrustatum* (Tables 4, 5).

360 Facies B is dominated by *P. aerugineo-caeruleum* and the corresponding phylotype
361 III. Sites with Facies C and/or a combination of Facies C and A are characterized by
362 populations of *P. incrustatum* and the corresponding phylotype I. Moreover, *P.*
363 *aerugineo-caeruleum*, and phylotype III, were also found in all those sites with Facies C
364 and/or with Facies C and A, although it was dominant only in site P11 (Tables 4, 5).

365

366 6.2. Cyanobacterial structures in different environments

367 Evidence from the deposits that formed on the tablets shows that the
368 cyanobacterial structures found in the fast-flowing areas, the slow-flowing areas, and
369 the stepped waterfalls and small waterfalls vary in accord with the dominant
370 cyanobacterial populations.

371

372 6.2.1. Stromatolites in fast-flowing water areas

373 The laminae in the stromatolites of Facies A, which dominates in this environment,
374 are formed largely of subperpendicular tube-shaped calcite bodies (Fig. 7A, B). The
375 tubes resulted from calcite precipitation around filamentous cyanobacteria that were
376 later lost to decay (e.g., as noted and explained by Merz-Preiß and Riding, 1999;
377 Golubić et al., 2008). The inner diameter of the tubes, from 6 to 7.5 μm , corresponds
378 to the diameter of *P. incrustatum*. The wall of these tubes, 2 to 12 μm thick, are
379 formed of calcite crystals, up to 6 μm long, that range in morphology from subhedral

380 to triangular-shaped to rhombohedral (Fig. 7B-E). Less porous fabrics developed in
381 areas where calcite was precipitated around groups of filaments (Fig. 7B). A variety of
382 diatoms and calcified EPS strands, along with morphologically variable calcite crystals
383 are common between the tubes (Fig. 7C, E).

384 *6.2.2. Uneven laminae/stromatolites and scattered cyanobacterial tubes in slow-*
385 *flowing water areas*

386 Facies B, which dominates in this environment, is characterized by laminae
387 formed of thin, discontinuous stromatolites, and isolated calcite tubes. Calcite tubes
388 formed by encrustation around cyanobacterial filaments are isolated (Fig. 8A), form
389 clusters of 4 to 6 tubes, form isolated domes, or develop uneven laminae with
390 randomly oriented tubes (Fig. 8B). In general, these tubes do not form clearly defined
391 laminae. Most of the calcite tubes have an inner diameter of 2.5 to 6.0 μm (most are 5
392 to 6 μm , which corresponds to the diameter of individual *P. aerugineo-caeruleum*
393 cells). The walls of the tubes, 3 to 8 μm thick, are formed of morphologically variable
394 calcite crystals (Fig. 8C, D). Varied pennate diatoms occur on and between the calcite
395 tubes (Fig. 8C, D). Other smaller calcite tubes (inner diameter of 1-3 μm), which are
396 scattered throughout, may belong to various species of *Leptolyngbya*.

397 *6.2.3. Stromatolites and irregular cyanobacterial masses formed in stepped waterfalls*
398 *and small waterfalls*

399 The two types of cyanobacterial structures found in this setting are as follows.

- 400 • Stromatolites (Facies A; Fig. 9A), up to 1.5 cm thick, interbedded with calcite-
401 coated moss and algal deposits (see Fig. 4C). Most are formed of calcite tubes that
402 have an inner diameter of 6-7.5 μm (*cf. P. incrustatum*) and calcite coatings 3-6

403 μm thick, in which crystal sizes and shapes are similar to those formed in fast-
404 flowing water areas devoid of macrophytes (Fig. 9B).

- 405 • Isolated and unevenly grouped cyanobacterial tubes that form irregular and
406 discontinuous masses (a) among the moss and macroscopic-alga calcite-coated
407 bodies, and (b) in the calcite coatings around the macrophytes. These masses are
408 formed of randomly oriented calcite tubes, uncoated bacterial filaments, diatoms,
409 and EPS strands (Fig. 9C, D). The calcite tubes that formed around the
410 cyanobacterial filaments have an inner diameter of 2.5-6 μm , and walls up to 10
411 μm thick that include numerous diatoms (Fig. 9D). The most abundant calcite
412 tubes, with an inner diameter of 5-6 μm , are assigned to *P. aerugineo-caeruleum*.
413 Some of the small diameter tubes may correspond to *Leptolyngbya* (Fig. 9D).

414 6.3. Cyanobacterial calcification

415 6.3.1. Calcification of *P. incrustatum*

416 *P. incrustatum* has been calcified to varying degrees (Fig. 10A-D). Some specimens
417 have small and dispersed groups of calcite crystals on their sheaths (Fig. 10A, B),
418 whereas other sheaths have an uneven calcite coating (Fig. 10C, D). Such coatings are
419 commonly thicker around the base of the filaments (Fig. 10D). The living trichomes
420 commonly vacated their sheaths, leaving behind empty tubes (Fig. 10D).

421 Different degrees of calcification are also evident in Facies A that formed on the
422 tablets that were placed in the areas of fast-flowing water devoid of macrophytes
423 (Figs. 7B-E, 10E-G), and in the stepped waterfalls and small waterfalls (Fig. 9B). In
424 these deposits, the calcite coatings around the filaments are 2 to 12 μm thick. Rare
425 calcified sheaths and filaments are also present (e.g., Fig. 7C). Most cross-sections

426 through the coatings show that there is no consistent pattern in terms of crystal size
427 and shape. In some cases, the coating is < 2 μm thick and formed of irregular,
428 anhedral, CaCO_3 nanoparticles (e.g., Fig. 10E). In some of the thicker coatings,
429 however, there is a change from smaller and/or irregular crystals (mainly subhedral) in
430 the inner part, to larger and/or well formed, chiefly rhombohedral and triangular-
431 shaped crystals outwards (Figs 7C-E, 5D, 10F, G).

432 Pennate diatoms and EPS strands remain attached to the filament coatings (Fig.
433 7C, E). Calcified EPS strands between tubes encompass subrhombohedral to anhedral
434 nanoparticles (Fig. 7E).

435 6.3.2. Calcification in other cyanobacteria

436 Encrustations around *P. aerugineo-caeruleum* tubes (inner diameters of 5-6 μm),
437 found in Facies B that formed on tablets placed in the areas of slow-flowing water
438 (Figs. 8B-D, 11A, B), are formed of a thin coating (3-4 μm thick) of subhedral to
439 rhombohedral crystals that are generally < 1 μm long (Figs 8C, D, 11A, B). In thicker
440 coatings, the crystals were more varied in size. In general, numerous diatoms and EPS
441 are associated with these tubes (Fig. 8C, D).

442 Calcification of the less common cyanobacteria species is more difficult to
443 ascertain because of their rarity and the fact that they did not form specific structures.
444 A variety of smaller tubes (inner diameter 1-3 μm), which may correspond to various
445 species of *Leptolyngbya*, was found in Facies B and C on the tablets placed in the slow
446 flowing areas and stepped waterfalls and small waterfalls. Such tubes, commonly
447 arranged in small groups (Fig. 9D), are typically formed of a wall (up to 4-5 μm thick)
448 that is formed of subhedral to rhombohedral calcite crystals of varied size (commonly

449 < 1 μm long), but commonly with rhombohedral crystals that increase in size outwards
450 (Fig. 11C, D).

451 **7. Discussion**

452 Molecular studies have shown that cyanobacterial diversity in tufas and
453 stromatolites that developed in freshwater and marine habitats varies in accord with
454 environmental conditions (Janssen et al., 1999; Reid et al., 2000; Arp et al., 2001, 2010;
455 Santos et al., 2010; Shiraishi et al., 2010; Bosak et al., 2012). Bacterial communities in
456 the River Piedra are dominated by cyanobacteria, with the filamentous Oscillatoriales
457 being the most common group, as shown by morphological and phylogenetic analyses.
458 In addition, a unicellular representative was recorded in both microscopic examination
459 and the sequence analysis. These filamentous cyanobacteria are typically preserved as
460 hollow tubes that formed through calcite encrustation around the filaments followed
461 by decay of the soft tissues. There are only rare examples where the filament and/or
462 sheath have been preserved through calcite impregnation (cf. Riding, 1991). Thus,
463 most of the stromatolites in these deposits are formed of laminae that are constructed
464 of hollow tubes. Cyanobacteria with similar styles of preservation are also found in the
465 non-laminated and poorly laminated deposits that form in the slow-flowing water
466 areas (Facies B) and in stepped waterfalls (Facies C). The cyanobacterial structures that
467 developed under slow flow conditions, however, do not form extensive or regularly
468 laminated deposits.

469 In the River Piedra, stromatolites (Facies A) in the fast-flowing water areas are
470 dominated by *P. incrustatum*. In contrast, *P. aerugineo-caeruleum* dominates in areas
471 that are characterized by Facies B that formed under low water velocity conditions.
472 Both species are found in the stepped waterfalls and small waterfalls. In this

473 environment, *P. incrustatum* dominates in zones with fast-flowing and strong vertical
474 water flow, where it constitutes Facies A, whereas *P. aerugineo-caeruleum* dominates
475 in zones with slow- to moderate-flowing water that are dominated by moss and algae
476 (Facies C). Other cyanobacteria (e.g., *Leptolyngbya*) are also present in the areas with
477 slow flowing water.

478
479 *7.1. Flow conditions and variations in cyanobacterial populations*

480 This and previous studies have suggested that the development of sedimentary
481 facies with variable deposition rates in the River Piedra are related to flow conditions,
482 which in turn, control the flora and bacteria and their calcification patterns (Vázquez-
483 Urbez et al., 2010; Arenas et al., 2014). In this river, cyanobacterial populations
484 dominated by *P. incrustatum* thrive in areas with shallow, fast-flowing water where
485 there is intense mechanical CO₂ outgassing, the highest deposition rates, and
486 laminated deposits. In contrast, cyanobacterial populations dominated by *P.*
487 *aerugineo-caeruleum* are found in areas with slow flowing water, where there is less
488 intense mechanical CO₂ outgassing, lower deposition rates, and the development of
489 poorly laminated deposits.

490 CO₂ uptake through photosynthesis is generally considered to be much less than
491 that of physical CO₂ outgassing, especially in high-CO₂ and/or fast flowing water
492 systems (Arp et al., 2001; Chen et al., 2004; Shiraisi et al., 2008, 2010). Arenas et al.
493 (2014) reached a similar conclusion for the River Piedra even though the precise
494 contribution of each type of CO₂ removal was unknown. Pentecost (1975), from
495 calculations based on rates of photosynthetic CO₂ uptake with ¹⁴C, argued that up to
496 20% of the calcification in *Rivularia* could be the direct result of photosynthesis. Mass

497 balance estimations in other European karst streams also indicated that in fast flowing,
498 shallow water, cyanobacterial photosynthesis accounts for 10–20% of the total Ca^{2+}
499 loss, with the remaining Ca^{2+} loss being caused by physicochemical precipitation
500 (Shiraishi et al., 2008; Arp et al., 2010; Pentecost and Franke, 2010). In these systems,
501 it therefore appears that photosynthesis exerts less influence on CaCO_3 precipitation
502 than the abiotic CO_2 evasion related to flow conditions. These results are consistent
503 with the results obtained in this study.

504 Although carbonate precipitation is not necessarily biologically driven, the
505 cyanobacteria do provide surfaces that are amenable to calcite precipitation
506 (Pentecost and Whitton, 2000). Specifically, it has been argued that various geochemical
507 properties of the surface of the sheath and the colony architecture of *P. incrustatum*
508 actively promotes the early stages of calcification (Pentecost and Whitton, 2000). Thus,
509 differences in the cyanobacteria, resulting from adaptive traits to cope with specific
510 environmental conditions, may explain some of the differences in calcification.
511 Therefore, in fluvial carbonate systems, if all other parameters are equal (e.g., water
512 composition, temperature, insolation), it is the depositional conditions (primarily flow
513 conditions) that control the distribution of the different cyanobacterial populations
514 and, in turn, the CaCO_3 precipitation processes that take place in each environment.

515 *7.2. Cyanobacterial structures: calcification, filament orientation, and lamination*

516 Calcification is a characteristic feature of many cyanobacteria, including
517 representatives of the Oscillatoriales such as *Phormidium*, *Lyngbya*, and *Plectonema*
518 (Zavarzin, 2002). It is important to note, however, that other cyanobacteria may
519 remain uncalcified even when exposed to waters with the same degree of CaCO_3
520 saturation (Brehm et al., 2006; Golubić et al., 2008). It is possible that species-specific

521 differences may play a role in determining many aspects of calcification, including
522 crystal shape, sheath impregnation, and encrustation around the filaments (Merz-Preiß
523 and Riding, 1999; Merz-Preiß, 2000; Jones and Peng, 2014).

524 The strong influence of depositional conditions on colonization patterns of
525 cyanobacteria in different environments of the River Piedra does not allow definitive
526 resolution of the species-specific attributes. Nevertheless, differences in the degree of
527 calcification associated with *P. incrustatum* (Fig. 10) may have resulted, at least in part,
528 from slight differences in parameters such as the CO₂ outgassing rates, temperature,
529 and Ca concentrations, that contribute to the calcite saturation index (Table 2), as has
530 been suggested by several authors (e.g., Pentecost, 2005; Pedley et al., 2009; Jones
531 and Peng, 2014).

532 Textural attributes of the deposits in the River Piedra indicate that flow conditions
533 exert a strong influence on filament orientation and calcification of the microbial mats.
534 In areas with rapid flow with intense CO₂ outgassing and high calcite saturation indices,
535 filaments of *P. incrustatum* are rapidly coated by CaCO₃ and their growth keeps pace
536 with calcification. This produces a tight, rigid structure that is formed largely of coated
537 filaments set subperpendicular to surface that can withstand the fast flow water.
538 Moreover, the dense filamentous mats formed by *P. incrustatum* increase the surface
539 area available for CaCO₃ precipitation and thereby increase resistance to water flow
540 (cf., Golubić et al., 2008). In the River Piedra, such rapid calcification may also favour
541 the formation of several laminae over a few months (Fig. 2C) that may, for example, be
542 related to short-term changes in flow rate. Slight variations in any of the
543 environmental parameters that affect the calcite saturation index in the carbonate
544 system may promote the formation of distinctive laminae (Guo and Riding, 1994).

545 Areas of the River Piedra with slow flowing water, where CO₂ outgassing is less
546 intense and CaCO₃ precipitation is slower, are characterized by cyanobacterial mats
547 that are dominated by *P. aerugineo-caeruleum*. Uneven laminae formed of randomly
548 oriented and less commonly subperpendicular tubes with open to dense fabrics are
549 interbedded with loose sediment. Features in these beds are consistent with the
550 slower precipitation of CaCO₃ around the filaments that is engendered by the slow
551 flowing deeper water that commonly has a lower calcite saturation index than found in
552 the fast flowing water (Table 2). These cyanobacterial mats, dominated by *P.*
553 *aerugineo-caeruleum*, do not form thick or extensively lateral deposits. Although these
554 mats may not build thick laminated deposits, they mediate deposition by trapping and
555 binding sediment to the substrate, thus enhancing cohesiveness of the loose sediment
556 (cf., Golubić et al., 2000; Seong-Joo et al., 2000; Noffke et al., 2003).

557 7.3. The role of EPS in calcification

558 EPS play an important role in microbial mat formation (Decho, 2000; Frank and
559 Belfort, 2003). Comparative studies of cyanobacteria have shown that *Phormidium* is
560 the highest producer of EPS (Nicolaus et al., 1999; Di Pippo et al., 2013). The high EPS
561 production associated with *P. incrustatum* in the River Piedra would contribute to the
562 better attachment to surfaces and permit growth in fast-flowing waters.

563 EPS has also been considered essential for providing mineral nucleation sites in
564 tufa-forming microbial mats in karst streams (Pentecost, 1985, 2005). EPS can remain
565 associated with the cell surface as sheaths and/or be released into the surrounding
566 environment (De Philippis and Vincenzini, 2003). EPS mediates CaCO₃ precipitation by
567 providing diffusion-limited microenvironments that create alkalinity gradients in
568 response to metabolic processes, and by attracting and binding Ca ions to negatively

569 charged sites (Arp et al., 2010).

570 In addition to variations in some of the parameters that affect the bulk saturation
571 index of water with respect to calcite, changes in calcite saturation levels in the
572 microbially produced EPS around the cells may also contribute to morphological
573 variations evident in calcite that forms around the microbes (e.g., Figs 7C-D, 8C, D, 9B,
574 10E-G, 11). Studies of *Scytonema julianum* encrustations in different geological and
575 geographic areas showed that there was a progressive change in crystal morphology
576 that was probably microbially controlled by microscale changes in the saturation levels
577 that developed in the EPS (Jones and Peng, 2014).

578 The outward increase in crystal size, which is a common feature of the tubes
579 that developed around many of the microbes (particularly *P. incrustatum*) found in the
580 River Piedra, may be due to the fact that the ongoing precipitation of CaCO₃ around
581 the microbes will progressively isolate the growth surface from microbial influence
582 (Jones and Peng, 2014). With this model, the larger crystals on the outermost surfaces
583 of the cyanobacterial tubes are probably related to the physiochemical conditions in
584 the surrounding water rather than in the EPS. The innermost part of the thick
585 encrusting layers and all of the thinner encrusting layers around *P. incrustatum*, *P.*
586 *aerugineo-caeruleum* and *Leptolyngbya* (Figs. 8D, 11B-D) are commonly formed of
587 small, irregularly shaped calcite crystals. This may reflect the fact that higher
588 saturation levels are expected around the cell walls (Jiménez-López et al., 2011). This
589 idea also suggests that in slow flowing water, precipitation may be more influenced by
590 metabolic processes associated with the EPS than in fast flowing water.

591

592 **8. Comparison with other carbonate fluvial systems**

593 Stromatolites made of cyanobacterial calcite tubes similar to those found in this
594 study have been described in other modern fluvial tufa systems (e.g., Merz-Preiß and
595 Riding, 1999; Arp et al., 2001, 2010; Golubić et al., 2008). *P. incrustatum* is the
596 dominant cyanobacterium in laminated deposits of some tufa-forming streams in
597 Belgium (Janssen et al., 1999), Germany (Merz-Preiß and Riding, 1999; Arp et al., 2001,
598 2010) and Japan (Shiraishi et al., 2010). In those examples, *P. incrustatum* was found in
599 fast-flowing water. Other cyanobacteria are also common in fast-flowing conditions of
600 other tufa systems (Golubić et al., 2008; Arp et al., 2010). For instance, in the Plitvice
601 system Golubić et al. (2008) identified *P. incrustatum*, *Schizothrix fasciculate*, *P.*
602 *favosum*, *P. uncinatum* and *Hydrocoleum homoeotrichum*, and *Rivularia haematites*. In
603 this example, species-specific differences in the degree of calcification and in the shape
604 of the resulting calcium carbonate crystals are apparent (Obenlußneschloss and
605 Schneider, 1991). In the River Piedra environments, similar variations evident between
606 the different environments can be attributed to differences in flow conditions and
607 associated hydrochemical parameters.

608 Most studies of fluvial stromatolites have focused on taxonomic questions,
609 phylogenetic relationships (Arp et al., 2010; Santos et al., 2010; Brinkmann et al.,
610 2015), composition of the stromatolite-forming mats (e.g., Arp et al., 2010), the
611 conditions under which cyanobacteria calcify (Merz-Preiß and Riding, 1999), or the
612 contribution of cyanobacterial photosynthetic CO₂-uptake to calcification (Arp et al.,
613 2010; Shiraishi et al., 2008, 2010). The cyanobacteria most frequently recovered in
614 these studies were Oscillatoriales, although representatives of unicellular genera were
615 also found. In general, however, the depositional structures and calcification of the
616 microbial constituents have not been related to variations in flow conditions or to

617 variations in depositional rates between different fluvial environments.

618 Merz-Preiß and Riding (1999) focused on conditions under which cyanobacteria
619 calcify and concluded that (1) the CO₂ content in water determines if filament
620 encrustation or sheath impregnation takes place, and (2) calcite encrustation is
621 conspicuous when the calcite saturation index > 0.8. They inferred that in fast-flowing
622 streams cyanobacteria utilize CO₂ in photosynthesis, whereas in sluggish water
623 cyanobacteria utilize HCO₃, which leads to sheath impregnation by CaCO₃ even where
624 calcite saturation index is only 0.2–0.3. Results from the River Piedra show that calcite
625 encrustation is the dominant process for cyanobacterial calcification in all settings
626 where the mean calcite saturation index is between *ca* 0.6 and 0.9 (Arenas et al.,
627 2014). In addition, data from the River Piedra indicate that variations in the crystal size,
628 crystal shape, and thickness of the encrustation may reflect the variable influence of
629 physicochemical conditions associated with EPS around the cells (cf., Jones and Peng,
630 2014). This may be more important to calcite precipitation in slow-flowing water than
631 in fast-flowing water.

632 This study has shown that the fluvial tufa environment contains morphologically
633 diverse and genetically recognizable cyanobacterial populations with the dominant
634 cyanobacterial communities being dependent on the depositional environmental
635 conditions (primarily water flow conditions). These factors are manifest in the distinct
636 textures and structures found in the associated facies. Therefore, the distinct
637 depositional structures (e.g., arrangement of calcite tubes) and calcification styles
638 (e.g., size and shape of crystals and thickness of encrustations) of the cyanobacterial
639 calcite tubes found in different sedimentary facies should be taken into account in
640 interpreting environmental conditions of ancient carbonate sedimentary systems.

641

642 9. Conclusions

643 Analysis of sedimentological attributes and cyanobacterial diversity in the River
644 Piedra in the Monasterio de Piedra Natural Park has produced the following important
645 conclusions.

- 646 • Morphological and phylogenetic analyses of living bacterial mats showed that the
647 distribution of the dominant cyanobacterial species is linked to flow conditions.
- 648 • *Phormidium incrustatum* dominates in the fast-flowing water where the mean
649 deposition rate is 1.6 cm/year. This taxon is responsible for the formation of
650 extensive, thick stromatolites that are formed largely of palisades of calcite tubes
651 that formed as a result of calcite encrustation around the living filaments.
- 652 • *Phormidium aerugineo-caeruleum* dominates in areas with slow-flowing water,
653 where it formed uneven laminae, and calcite tubes that are scattered throughout
654 the loose, structureless sediments, that accumulated at 0.3 cm/yr. Although this
655 species tends not to form stromatolites, it does contribute to the cohesiveness of
656 the loose sediment.
- 657 • *P. incrustatum* and *P. aerugineo-caeruleum* are found in stepped waterfalls and
658 small waterfalls environments where they are associated with the spongy moss
659 and algal boundstone.
- 660 • The calcite encrustations that form around the cyanobacteria do not typically
661 exhibit regular patterns. This may be a reflection of changes in the parameters
662 that affect the calcite saturation index. The change in shape and size of the CaCO₃
663 precipitates may be more strongly influenced by the physicochemical conditions
664 in the EPS around the cells than by the chemical characteristics of the river water.

665 These metabolic processes may be more significant to calcite precipitation in
666 slow-flowing water than in fast-flowing water.

- 667 • In fluvial carbonate systems it is the depositional conditions (primarily physical
668 flow conditions) that controls the cyanobacterial populations and the calcium-
669 carbonate precipitation processes in each environment.
- 670 • The varying cyanobacterial structures and calcification styles are significant
671 attributes that can be used to assess changes in depositional conditions of
672 ancient carbonate sedimentary systems.

673 **Acknowledgments**

674 This study was funded by projects CGL2009-09216/CLI, CGL2013-42867-P and
675 CGL2013-44870-R of the Spanish Government and European Regional Funds. This
676 study forms part of the activities of the research group “Continental Sedimentary
677 Basins Analysis” (Aragón Government and University of Zaragoza). We are grateful to
678 the personnel of the *Servicio de Preparación de Rocas y Materiales Duros* and SEM
679 (*Servicio General de Apoyo a la Investigación-SAI*) of the University of Zaragoza, and
680 SEM of the University of Alberta, for their technical help. We thank the management
681 and staff of the Monasterio de Piedra Natural Park for facilitating our fieldwork. The
682 reviewers and editor are thanked for providing critical views that helped improve the
683 manuscript.

684

685 **REFERENCES**

- 686 Anagnostidis, K., Komárek, J. 1988. Modern approach to the classification system of
687 cyanophytes. 3. Oscillatoriales. *Archiv für Hydrobiologie, Supplement* 80, 327-472.
- 688 Arenas, C., Vázquez-Urbez, M., Auqué, L., Sancho, C., Osácar, C., Pardo, G., 2014.
689 Intrinsic and extrinsic controls of spatial and temporal variations in modern fluvial
690 tufa sedimentation: A thirteen-year record from a semi-arid environment.
691 *Sedimentology* 61, 90-132.
- 692 Arp, G., Wedemeyer, N., Reitner, J., 2001. Fluvial tufa formation in a hard-water creek
693 (Deinschwanger Bach, Franconian Alb, Germany). *Facies* 44, 1–22.
- 694 Arp, G., Bissett, A., Brinkmann, N., Cousin, S., De Beer, D., Friedl, T., Mohr, K.I., Neu,
695 T.R., Reimer, A., Shiraishi, F., Stackebrandt, E., Zippel, B., 2010. Tufa-forming
696 biofilms of German karstwater streams: microorganisms, exopolymers,
697 hydrochemistry and calcification. In: Pedley, H.M., Rogerson, M. (Eds.), *Tufas and*
698 *Speleothems: Unravelling the Microbial and Physical Controls*. Geological Society,
699 London, Special Publication 336, pp. 83–118.
- 700 Awramik, S.M., 1991. Archaean and Proterozoic Stromatolites. In: Riding, R. (Ed.)
701 *Calcareous Algae and Stromatolites*. Springer-Verlag, Berlin, pp. 290-304.
- 702 Beraldi-Campesi, H., Arenas-Abad, C., Garcia-Pichel, F., Arellano-Aguilar, O., Auque, L.,
703 Vazquez-Urbez, M., Sancho, C., Osacar, C., Ruiz-Velasco, S., 2012. Benthic bacterial
704 diversity from freshwater tufas of the Iberian Range (Spain). *FEMS Microbiology*
705 *Ecology* 80, 363-379.

706 Berrendero, E., Perona, E., Mateo, P., 2008. Genetic and morphological
707 characterization of *Rivularia* and *Calothrix* (Nostocales, Cyanobacteria) from
708 running water. *International Journal of Systematic and Evolutionary Microbiology*
709 58, 447-460.

710 Bosak, T., Liang, B., Wu, T.D., Templer, S.P., Evans, A., Vali, H., Querquin-Kern, J.L.,
711 Klepac-Ceraj, V., Sim, M.S., Mui, J., 2012. Cyanobacterial diversity and activity in
712 modern conical stromatolites. *Geobiology* 10, 384-401.

713 Brehm, U., Krumbein, W.E., Palinska, K.A., 2006. Biomicrospheres generate ooids in the
714 laboratory. *Geomicrobiology Journal* 23, 545–550.

715 Brinkmann, N., Hodač, L., Mohr, K. I., Hodačová, A., Jahn, R., Ramm, J., Hallmann, C.,
716 Arp, G., Friedl, T., 2015. Cyanobacteria and Diatoms in Biofilms of Two Karstic
717 Streams in Germany and Changes of Their Communities Along Calcite Saturation
718 Gradients. *Geomicrobiology Journal* 32, 255-274.

719
720 Burne, R.V., Moore, L.S., 1987. Microbialites: organosedimentary deposits of benthic
721 microbial communities. *Palaios* 2, 241–254.

722 Chen, J., Zhang, D.D., Wang, S., Xiao, T., Huang, R., 2004. Factors controlling tufa
723 deposition in natural waters at waterfall sites. *Sedimentary Geology* 166, 353–366.

724 Decho, A.W., 2000. Microbial biofilms in intertidal systems: an overview. *Continental*
725 *Shelf Research* 20, 1257–1273.

726 De Philippis, R., Vincenzini, M., 2003. Outermost polysaccharidic investments of
727 cyanobacteria: nature, significance and possible applications. *Recent Research*
728 *Developments in Microbiology* 7, 13-22.

729 Di Pippo, F., Ellwood, N.T.W., Gismondi, A., Bruno, L., Rossi, F., Magni, P., De Philippis,
730 R., 2013. Characterization of exopolysaccharides produced by seven biofilm-
731 forming cyanobacterial strains for biotechnological applications. *Journal of Applied*
732 *Phycology* 25, 1697-1708.

733 Edwards, U., Rogall, T., Blöcker, H., Emde, M., Böttger, E.C., 1989. Isolation and direct
734 complete nucleotide determination of entire genes. Characterization of a gene
735 coding for 16S ribosomal RNA. *Nucleic Acids Research* 17, 7843–7853.

736 Frank, B.P., Belfort, G., 2003. Polysaccharides and sticky membrane surfaces: critical
737 ionic effects. *Journal of Membrane Science* 212, 205-212.

738 Gkelis, S., Rajaniemi, E., Vardaka, M., Moustaka-Gouni, M., Lanaras, T., Sivonen, K.,
739 2005. *Limnothrix redekei* (Van Goor) Meffert (Cyanobacteria) strains from lake
740 Kastoria, Greece from a separate phylogenetic group. *Microbial Ecology* 49, 176–
741 182.

742 Golubić, S., Seong-Joo, L., Browne, K.M., 2000. Cyanobacteria: Architects of
743 Sedimentary Structures. In: Riding, R.E., Awramik, S.M. (Eds.), *Microbial Sediments*.
744 Springer-Verlag, Berlin, pp. 57-67.

745 Golubić, S., Violante, C., Plenković–Moraj, A., Grgasović, T., 2008. Travertines and
746 calcareous tufa deposits: an insight into diagenesis. *Geologia Croatica* 61, 363–378.

747 Gomont, M., 1892 '1893'. Monographie des Oscillariées (Nostocacées Homocystées).
748 Deuxième partie. - Lyngbyées. *Annales des Sciences Naturelles, Botanique, Série 7*
749 16, 91-264.

750 Gradziński, M., 2010. Factors controlling growth of modern tufa: results of a field
751 experiment. In: Pedley, P.M., Rogerson, M. (Eds.), *Tufas and Speleothems:*
752 *Unravelling the Microbial and Physical Controls.* Geological Society, London, Special
753 Publication 336, pp. 143–191.

754 Guo, L., Riding, R., 1994. Origin and diagenesis of Quaternary travertine shrub fabrics,
755 Rapolano Terme, central Italy. *Sedimentology* 41, 499-520.

756 Hall, T.A., 1999. BioEdit: a user-friendly biological sequence alignment editor and
757 analysis program for Windows 95/98/NT. *Nucleic Acids Symposium Series* 41, 95–
758 98.

759 Janssen, A., Swennen, R., Podoor, N., Keppens, E., 1999. Biological and diagenetic
760 influence in Recent and fossil tufa deposits from Belgium. *Sedimentary Geology*
761 126, 75–95.

762 Jiménez-López, C., Ben Chekroun, K., Jroundi, F., Rodríguez-Gallego, M., Arias, J.M.,
763 González-Muñoz, M.T., 2011. *Myxococcus xanthus* Colony Calcification: A study to
764 Better Understand the Processes Involved in the Formation of this Stromatolite-
765 Like Structure. In: Reitner, J., Quéric, N.V., Arp, G. (Eds.), *Advances in Stromatolite*
766 *Geobiology.* Lecture Notes in Earth Sciences. Springer-Verlag, Berlin, pp. 161–181.

767 Jones, B., Peng, X., 2014. Multiphase calcification associated with the atmophytic
768 cyanobacterium *Scytonema julianum*. *Sedimentary Geology* 313, 91-104.

769 Jukes, T.H., Cantor, C.R., 1969. Evolution of protein molecules. In: Munro, H.N. (Ed.),
770 *Mammalian Protein Metabolism.* Academic Press, New York, pp. 22–132.

771 Katoh, K., Standley, D.M., 2013. MAFFT multiple sequence alignment software version
772 7: improvements in performance and usability. *Molecular Biology Evolution* 30,
773 772–780.

774 Komárek, J., Anagnostidis, K., 1998. Cyanoprokaryota. 1. Teil: Chroococcales. In: Ettl,
775 H., Gärtner, G., Heynig, H., Mollenhauer, D. (Eds.), *Süßwasserflora von*
776 *Mitteleuropa*, 19/1). Spektrum Akademischer Verlag, Heidelberg, Berlin, 548 pp.

777 Komárek, J., Anagnostidis, K., 2005. Cyanoprokaryota, part 2. Oscillatoriales. In: Büdel,
778 B., Gärtner, G., Krienitz, L., Schagerl, M. (Eds.), *Süßwasserflora von Mitteleuropa*
779 *Band 19/2*. Elsevier/Spektrum, Heidelberg, 759 pp.

780 Krumbein, W.E., Brehm, U., Gerdes, G, Gorbushina, A.A., Levit, G., 2003. Biofilm,
781 biodictyon and biomat – biolaminites, oolites, stromatolites –g eophysiology,
782 global mechanism, parahistology. In: Krumbein, W.E., Paterson, D.M., Zavarzin,
783 G.A. Eds.), *Fossil and Recent Biofilms*. Kluwer, Dordrecht, pp. 1-27.

784 Lepère, C., Wilmotte, A., Meyer, B., 2000. Molecular diversity of *Microcystis* strains
785 (Cyanophyceae, Chroococcales) based on 16S rDNA sequences. *Systematics and*
786 *Geography of Plants* 70, 275–283.

787 Loza, V., Perona, E., Carmona, J., Mateo, P., 2013. Phenotypic and genotypic
788 characteristics of *Phormidium*-like cyanobacteria inhabiting microbial mats are
789 correlated with the trophic status of running waters. *European Journal of*
790 *Phycology* 48, 235-252.

791 Manzo, E., Perri, E., Tucker, M.E., 2012. Carbonate deposition in a fluvial tufa system:
792 processes and products (Corvino Valley – southern Italy). *Sedimentology* 59, 553–
793 577.

794 Merz-Preiß, M., 1992. The Biology of Carbonate Precipitation by Cyanobacteria. *Facies*
795 26, 81-102.

796 Merz-Preiß, M., 2000. Calcification in cyanobacteria. In: Riding, R.E., Awramik, S.M.
797 (Eds.), *Microbial Sediments*. Springer-Verlag, Berlin, pp. 50– 56.

798 Merz-Preiß, M., Riding, R., 1999. Cyanobacterial tufa calcification in two freshwater
799 streams: ambient environment, chemical thresholds and biological processes.
800 *Sedimentary Geology* 126,103–124.

801 Neu, T.R., 1996. Significance of bacterial surface-active compounds in interaction of
802 bacteria with interfaces. *Microbiological Reviews* 60, 151–166.

803 Nicolaus, B., Panico, A., Lama, L., Romano, I., Manca, M.C., De Giulio, A., Gambacorta,
804 A., 1999. Chemical composition and production of exopolysaccharides from
805 representative members of heterocystous and non-heterocystous cyanobacteria.
806 *Phytochemistry* 52, 639-647.

807 Noffke, N., Gerdes, G., Klenke, T., 2003. Benthic cyanobacteria and their influence on
808 the sedimentary dynamics of peritidal depositional systems (siliciclastic, evaporitic
809 salty, and evaporitic carbonatic). *Earth-Science Reviews* 62, 163-176.

810 Obenluånneschloss, J. and Schneider, J., 1991. Ecology and calcification patterns of
811 *Rivularia* (Cyanobacteria). *Archiv für Hydrobiologie, Supplementband 92*
812 (*Algological Studies* 64), 489–502.

813 Pedley, H.M., Rogerson, M., Middleton, R., 2009. Freshwater calcite precipitates from
814 in vitro mesocosm flume experiments: a case for biomediation of tufas.
815 *Sedimentology* 56, 511–527.

- 816 Pentecost, A., 1975. Calcium carbonate deposition and blue-green algae. PhD thesis.
817 University of Wales (UK).
- 818 Pentecost, A., 1985. Association of cyanobacteria with tufa deposits: identity,
819 enumeration, and nature of the sheath material revealed by histochemistry.
820 *Geomicrobiology Journal* 4, 285–298.
- 821 Pentecost, A., 2005. *Travertine*. Springer-Verlag, Berlin, 445 pp.
- 822 Pentecost, A., Whitton, B.A., 2000. Limestones. In: Whitton, B.A., Potts, M. (Eds.), *The*
823 *Ecology of Cyanobacteria*). Kluwer, Dordrecht, pp. 257–279.
- 824 Pentecost, A., Franke, U., 2010. Photosynthesis and calcification of the stromatolitic
825 freshwater cyanobacterium *Rivularia*. *European Journal of Phycology* 45, 345-353.
- 826 Reid, R.P., Visscher, P.T., Decho, Q.W., Stolz, J.K., Bebout, B.M., Dupraz, C., Macintyre,
827 I.G., Paerl, H.W., Pinckney, J.L., Prufert-Bebout, L., Steppe, T.F., Des Marais, D.J.,
828 2000. The role of microbes in accretion, lamination and early lithification of
829 modern marine stromatolites. *Nature* 406, 989–992.
- 830 Riding, R., 1991. Classification of Microbial Carbonates. In: Riding, R. (Ed.), *Calcareous*
831 *Algae and Stromatolites*. Springer-Verlag, Berlin, pp. 21-51.
- 832 Riding, R., 2000. Microbial carbonates: the geological record of calcified bacterial-algal
833 mats and biofilms. *Sedimentology* 47, 179–214.
- 834 Rosenberg, E., 1989. Biofilms on water-soluble substrates. In: Characklis, W.G.,
835 Wilderer, P.A. (Eds.), *Structure and Function of Biofilms*. Wiley, Chichester, UK, pp.
836 59–72.

837 Santos, F., Pena, A., Nogales, B., Soria-Soria, E., García del Cura, M.A., González-Martín,
838 J.A., Antón, J., 2010. Bacterial diversity in dry modern freshwater stromatolites
839 from Ruidera Pools Natural Park, Spain. *Systematic and Applied Microbiology* 33,
840 209-221.

841 Schopf, P., 2012. The Fossil Record of Cyanobacteria. In: Whitton, B. (Ed.), *Ecology of*
842 *Cyanobacteria II. Their diversity in space and time*. Springer, London, pp 15–36.

843 Seong-Joo, L, Browne, K.M., Golubić, S., 2000. On stromatolite lamination. In: Riding,
844 R.E., Awramik, S.M. (Eds.), *Microbial Sediments*. Springer-Verlag, Berlin, pp. 16-24.

845 Shiraishi, F., Reimer, A., Bisset, A., de Beer, D., Arp, G., 2008. Microbial effects on
846 biofilm calcification, ambient water chemistry and stable isotope records in a highly
847 supersaturated setting (Westerhöfer Bach, Germany). *Palaeogeography,*
848 *Palaeoclimatology, Palaeoecology* 262, 91–106.

849 Shiraishi, F., Okumura, T., Takahashi, Y., Kano, A., 2010. Influence of microbial
850 photosynthesis on tufa stromatolite formation and ambient water chemistry, SW
851 Japan. *Geochimica et Cosmochimica Acta* 74, 5289-5304.

852 Stolz, J.F., 2000. Structure of microbial mats and biofilms. In: Riding, R.E., Awramik,
853 S.M. (Eds.), *Microbial sediments*. Springer-Verlag, Berlin, pp. 1–8.

854 Tamura, K., Stecher, G., Peterson, D., Filipski, A., Kumar, S., 2013. MEGA6: Molecular
855 evolutionary genetics analysis version 6.0. *Molecular Biology and Evolution* 30,
856 2725–2729.

857 Tavaré, S., 1986. Some probabilistic and statistical problems in the analysis of DNA
858 sequences. Lectures on Mathematics in the Life Sciences. American Mathematical
859 Society 17, 57–86.

860 Vázquez-Urbez, M., Arenas, C., Sancho, C., Osácar, C., Auqué, L., Pardo, G., 2010.
861 Factors controlling present-day tufa dynamics in the Monasterio de Piedra Natural
862 Park (Iberian Range, Spain): depositional environmental settings, sedimentation
863 rates and hydrochemistry. *International Journal of Earth Sciences* 99, 1027–1049.

864 Whitton, B.A., 2011. Phylum Cyanophyta (Cyanobacteria). In: John, D.M., Whitton,
865 B.A., Brook, A.J. (Eds.), *The Freshwater Algal Flora of the British Isles. An
866 Identification Guide to Freshwater and Terrestrial Algae*. Cambridge University
867 Press, Cambridge, pp. 31–158.

868 Wright, E.S., Safak Yilmaz, L., Noguera, D.R., 2012. DECIPHER, A Search-Based Approach
869 to Chimera Identification for 16S rRNA Sequences. *Applied and Environmental
870 Microbiology* 78, 717-725.

871 Zavarzin, G.A., 2002. Microbial geochemical calcium cycle. *Mikrobiologija* 71, 5-22.

872

873

874 **FIGURE CAPTIONS**

875

876 **Fig. 1.** (A) Location of Monasterio de Piedra Natural Park and geological map of the
877 region. (B) Location of studied sites and the main waterfalls along the River Piedra
878 (modified from Arenas et al., 2014).

879 **Fig. 2.** Fast-flowing water environment and corresponding sedimentary facies
880 (stromatolites, Facies A). (A) Field view. (B) Plan view of stromatolite with knobby
881 surface. (C) Cross-section of stromatolite formed on a tablet in fast-flowing water
882 areas. The six-month periods are indicated: “Warm” corresponds to April–
883 September and “Cool” to October–March. (D) Optical microscope image of
884 stromatolite formed on a tablet. Lamination consisting of laminae with tight
885 filamentous cyanobacterial calcite bodies subperpendicular with respect to the
886 growth surface. Note voids formed by aquatic insects and worms.

887 **Fig. 3.** Slow-flowing water environment developed upstream of a small waterfall,
888 (loose lime mud and carbonate sediment, Facies B). (A) Field view. (B, C) Plan views
889 of deposit showing grayish-blue color of the cyanobacterial mat. (D) Cross-section
890 of deposit formed on a tablet; note that lamination is poor and mostly
891 characterized by the presence of thin white laminae. (E) Optical microscope image
892 of deposit formed on a tablet. Typical loose, structureless sediment consisting of
893 micrite with allochemical components (sections of calcite coated algae and
894 macrophytes). Note presence of a micrite mass made of elongated bodies that
895 resemble filamentous cyanobacteria (Cy).

896 **Fig. 4.** Stepped waterfall environment (moss, macroscopic algae, grass and
897 cyanobacterial mats; Facies C). (A) Field view. Tablet, installed for determining

898 deposition rates, is located at the bottom left of the image. (B) Detail of surface in
899 A, showing moss, algae and cyanobacterial mats. (C) Cross-section of deposit
900 formed on a tablet, consisting of moss and macroscopic-alga boundstone (Facies
901 C), associated with a stromatolite deposit at the base (Facies A). (D) Optical
902 microscope image of deposit formed on a tablet. Association of stromatolite
903 (laminae with tight filamentous cyanobacterial bodies, Cy) and boundstone
904 consisting of coated filamentous algae (cross sections, Al (tu)).

905 **Fig. 5.** Phylogenetic tree based on 16S rRNA gene sequences (1,315 positions) obtained
906 by the neighbor-joining method. Bootstrap support from neighbor-joining and
907 maximum likelihood analysis is reported above the nodes ($\geq 50\%$). I-IV are the
908 clusters in which sequences from this study are included. Sequences from this
909 study are indicated in bold and their associated GenBank accession numbers are
910 listed in Table 3. GenBank accession numbers for database sequences are in
911 parentheses following their name. The scale bar indicates 0.02 mutations per
912 nucleotide position.

913 **Fig. 6.** Light and fluorescence microscopy photomicrographs showing the main
914 cyanobacterial morphotypes identified in the samples. (A, B) *Phormidium*
915 *incrustatum*; (C) *Phormidium aerugineo-caeruleum*; (D, E) *Phormidium* sp.; (F)
916 *Leptolyngbya truncata*; (G, H) *Leptolyngbya foveolarum*; (I, J) *Leptolyngbya* sp.; (K,
917 L) *Chamaesiphon* sp. Scale bars = 20 μm .

918 **Fig. 7.** Scanning electron microscope images of samples selected from stromatolites
919 (Facies A) in which the dominant species is *Phormidium incrustatum*. (A, B) Calcite
920 tubes formed around *P. incrustatum*, with dominant subvertical orientation and
921 different degrees of calcification, with abundant EPS (in A). (C–E) Detail of calcite

922 tubes formed around *P. incrustatum*, with abundant calcified EPS in E. Note the
923 preserved calcified sheath (Sh) and abundant diatoms (Di) in C.

924 **Fig. 8.** Scanning electron microscope images of samples from deposits formed on
925 tablets installed in Facies B. (A) Typical loose, structureless sediment consisting of
926 isolated and clumped calcite crystals, diatoms and cyanobacterial tubes (arrow). (B)
927 Randomly oriented calcite tubes formed around cyanobacteria. (C, D) Calcite tubes,
928 probably formed around *Phormidium aerugineo-caeruleum*, consisting of small
929 calcite crystals (< 1 μm) and attached small diatoms. Note diatoms around the
930 tubes and EPS between tubes in D.

931 **Fig. 9.** Scanning electron microscope images of samples from deposits formed on
932 tablets installed in Facies C. (A) Mostly subvertical calcite tubes around *Phormidium*
933 *incrustatum* in stromatolite formed in a fast-flowing water zone. (B) Detail of
934 calcite tube in A. (C) Calcite crystals associated with EPS and cyanobacterial tubes.
935 (D) Randomly oriented calcite tubes, probably corresponding to *Leptolyngbya* sp.,
936 consisting of thick calcite coatings containing attached diatoms. Note EPS
937 (Extracellular Polymeric Substances) around the tubes. Cy (tu): Cyanobacteria
938 (tubes); Di: Diatoms.

939 **Fig. 10.** (A–D) Optical microscope images of *Phormidium incrustatum* showing different
940 degrees of calcification (samples taken on site from surface living mat). Explanation
941 in the text. (E–G) SEM images of samples selected from deposits formed on tablets
942 in fast-flowing water areas, showing calcite/ CaCO_3 coatings formed around
943 *Phormidium incrustatum*. (E) Thin coating formed of irregular (anhedral) and small
944 CaCO_3 forms. (F, G) Thick coatings showing larger crystals on outer part of coating.

945 **Fig. 11.** Scanning electron microscope images of samples selected from deposits
946 formed on tablets in slow flowing water areas. (A, B) CaCO₃ coatings formed
947 around *Phormidium aerugineo-caeruleum*. Note the small and irregular CaCO₃
948 forms throughout the coating. (C, D) CaCO₃ coatings formed around *Lyptolyngbya*
949 sp. Note in C the smaller size and irregular CaCO₃ forms in the interior and size
950 increase of rhombohedra outwards.

1
2
3
4
5
6
7
8
9
10
11
12
13
14
15
16
17
18
19
20
21
22
23
24
25
26
27
28
29
30
31
32
33
34
35
36
37
38
39
40
41
42
43
44
45
46
47
48
49
50
51
52
53
54
55
56
57
58
59
60

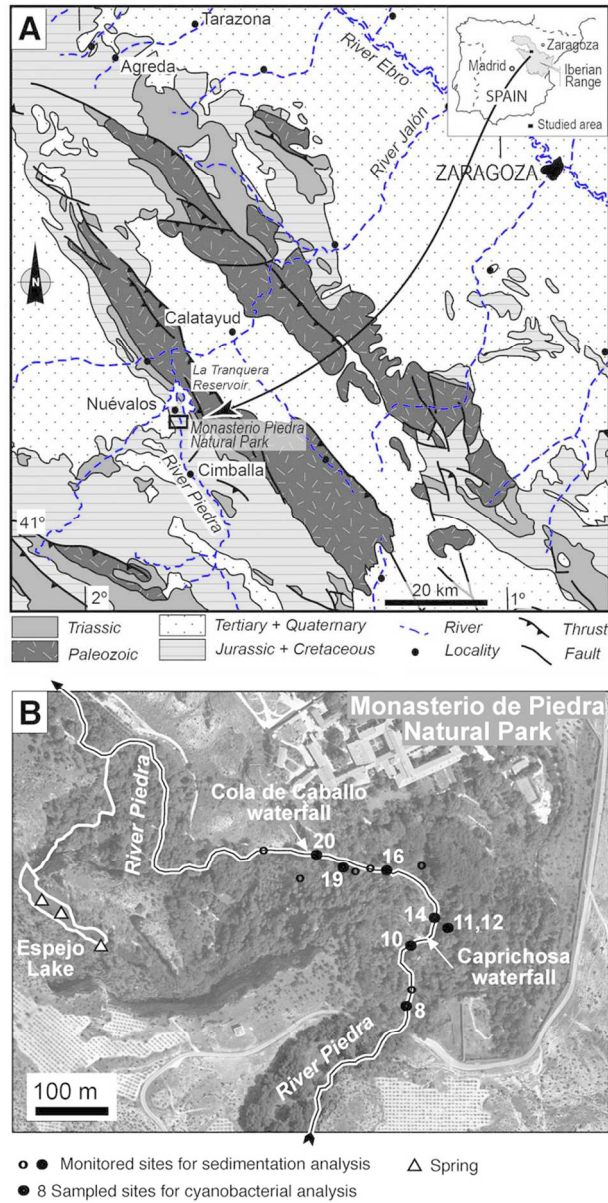


Fig. 1. (A) Location of the Monasterio de Piedra Natural Park and geological map of the region. (B) Location of studied sites, indicating the sites sampled for cyanobacterium analysis, and the main waterfalls along the River Piedra (modified from Arenas et al., 2014).
78x155mm (250 x 250 DPI)

1
2
3
4
5
6
7
8
9
10
11
12
13
14
15
16
17
18
19
20
21
22
23
24
25
26
27
28
29
30
31
32
33
34
35
36
37
38
39
40
41
42
43
44
45
46
47
48
49
50
51
52
53
54
55
56
57
58
59
60

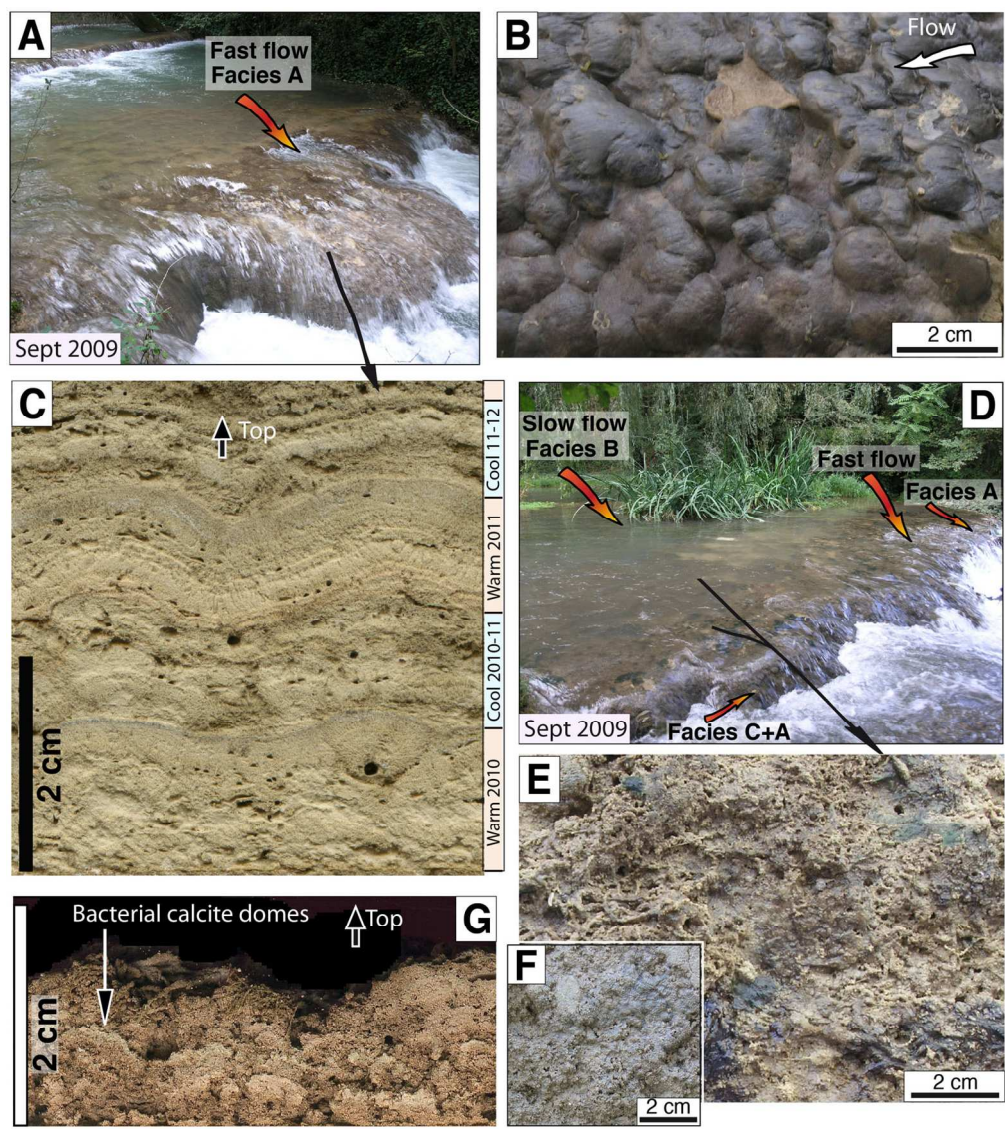


Fig. 2. (H) Stepped waterfall with moss, macroscopic algae, grass and cyanobacterial mats. The tablet installed for controlling deposition rate is located at the bottom left of the image. (I) Detail of surface in H, showing moss, algae and cyanobacterial mats. (J) Plan view of deposit in H showing stromatolite (hard calcified cyanobacterial mat) and calcite coated moss. (K) Cross-section of deposit formed on a tablet in the stepped waterfall shown in H, consisting of moss and macroscopic algal boundstone (facies C), associated with a stromatolite deposit at the base (facies A).
170x191mm (250 x 250 DPI)

1
2
3
4
5
6
7
8
9
10
11
12
13
14
15
16
17
18
19
20
21
22
23
24
25
26
27
28
29
30
31
32
33
34
35
36
37
38
39
40
41
42
43
44
45
46
47
48
49
50
51
52
53
54
55
56
57
58
59
60

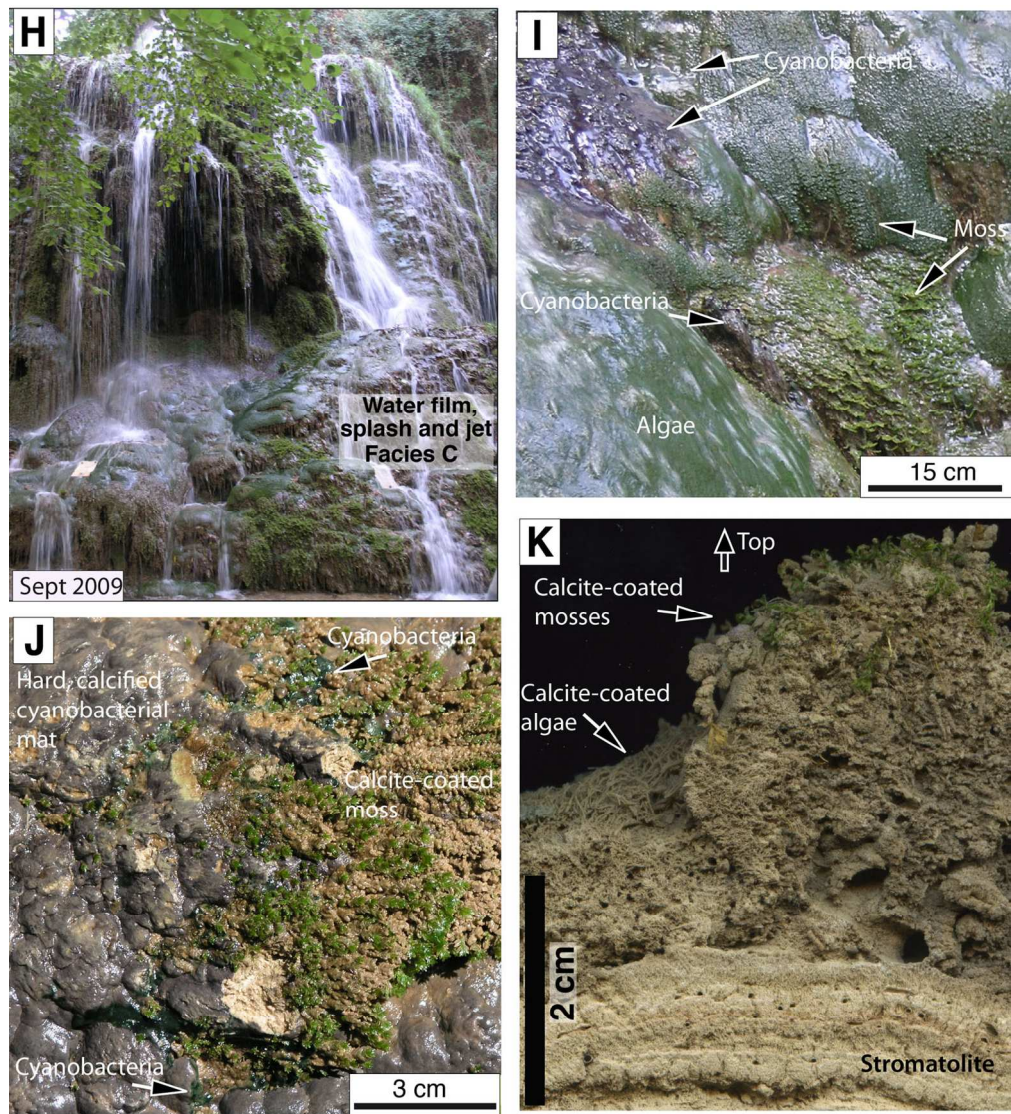


Fig. 2. (H) Stepped waterfall with moss, macroscopic algae, grass and cyanobacterial mats. The tablet installed for controlling deposition rate is located at the bottom left of the image. (I) Detail of surface in H, showing moss, algae and cyanobacterial mats. (J) Plan view of deposit in H showing stromatolite (hard calcified cyanobacterial mat) and calcite coated moss. (K) Cross-section of deposit formed on a tablet in the stepped waterfall shown in H, consisting of moss and macroscopic algal boundstone (facies C), associated with a stromatolite deposit at the base (facies A).
170x189mm (250 x 250 DPI)

1
2
3
4
5
6
7
8
9
10
11
12
13
14
15
16
17
18
19
20
21
22
23
24
25
26
27
28
29
30
31
32
33
34
35
36
37
38
39
40
41
42
43
44
45
46
47
48
49
50
51
52
53
54
55
56
57
58
59
60

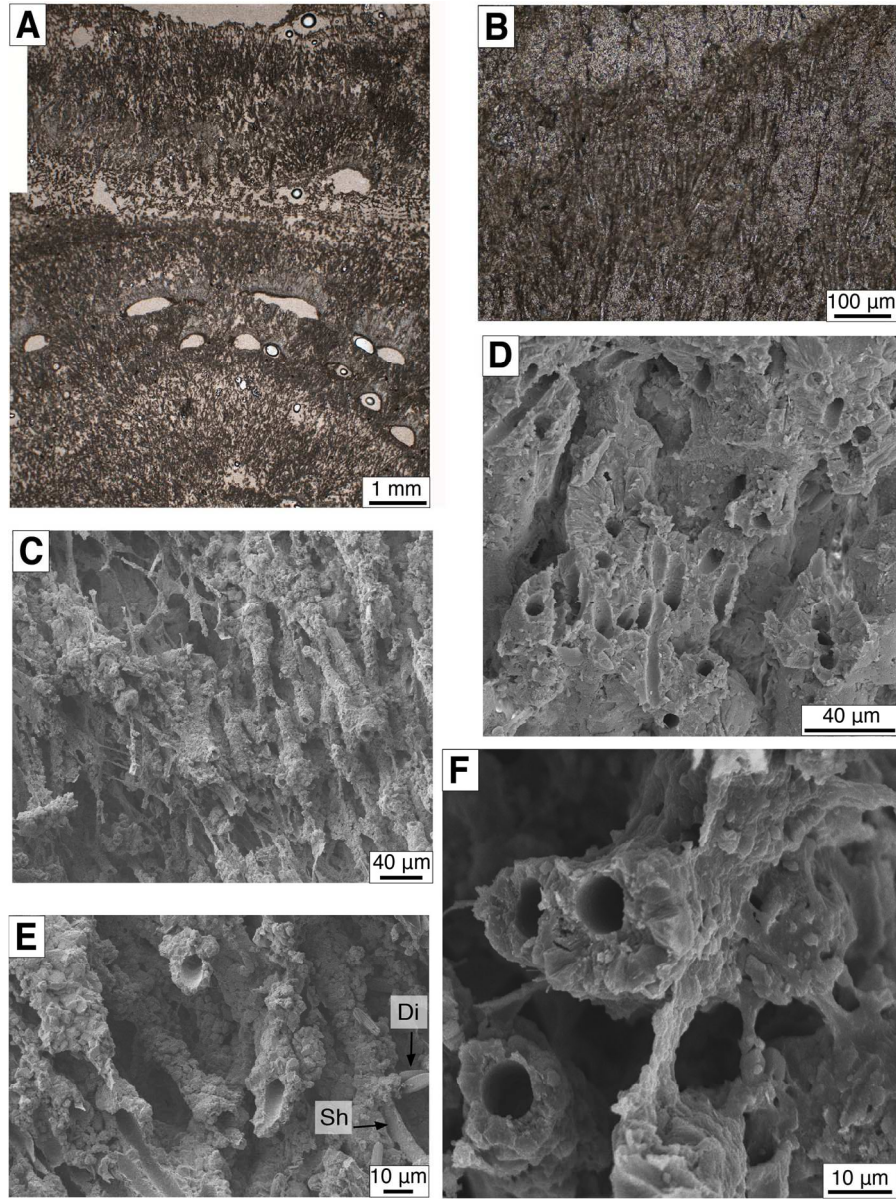


Fig. 3. Optical and scanning electron microscope images of samples selected from stromatolites (Facies A) formed on tablets installed in fast-flowing water areas. (A) Lamination consisting of laminae with tight filamentous cyanobacterial bodies subperpendicular with respect to the growth surface. Note voids from aquatic insects and worms. (B) Detail of filamentous cyanobacterial bodies. (C) and (D) Calcite tubes with dominant subvertical orientation and different degrees of calcification, with abundant EPS in A. (E) and (F) Detail of calcite tubes, with abundant calcified EPS in F. Note the preserved sheath (Sh) and the abundance of diatoms (Di) in E. Inner diameter of tubes in D to F is 6.5-7 μm.
169x228mm (250 x 250 DPI)

1
2
3
4
5
6
7
8
9
10
11
12
13
14
15
16
17
18
19
20
21
22
23
24
25
26
27
28
29
30
31
32
33
34
35
36
37
38
39
40
41
42
43
44
45
46
47
48
49
50
51
52
53
54
55
56
57
58
59
60

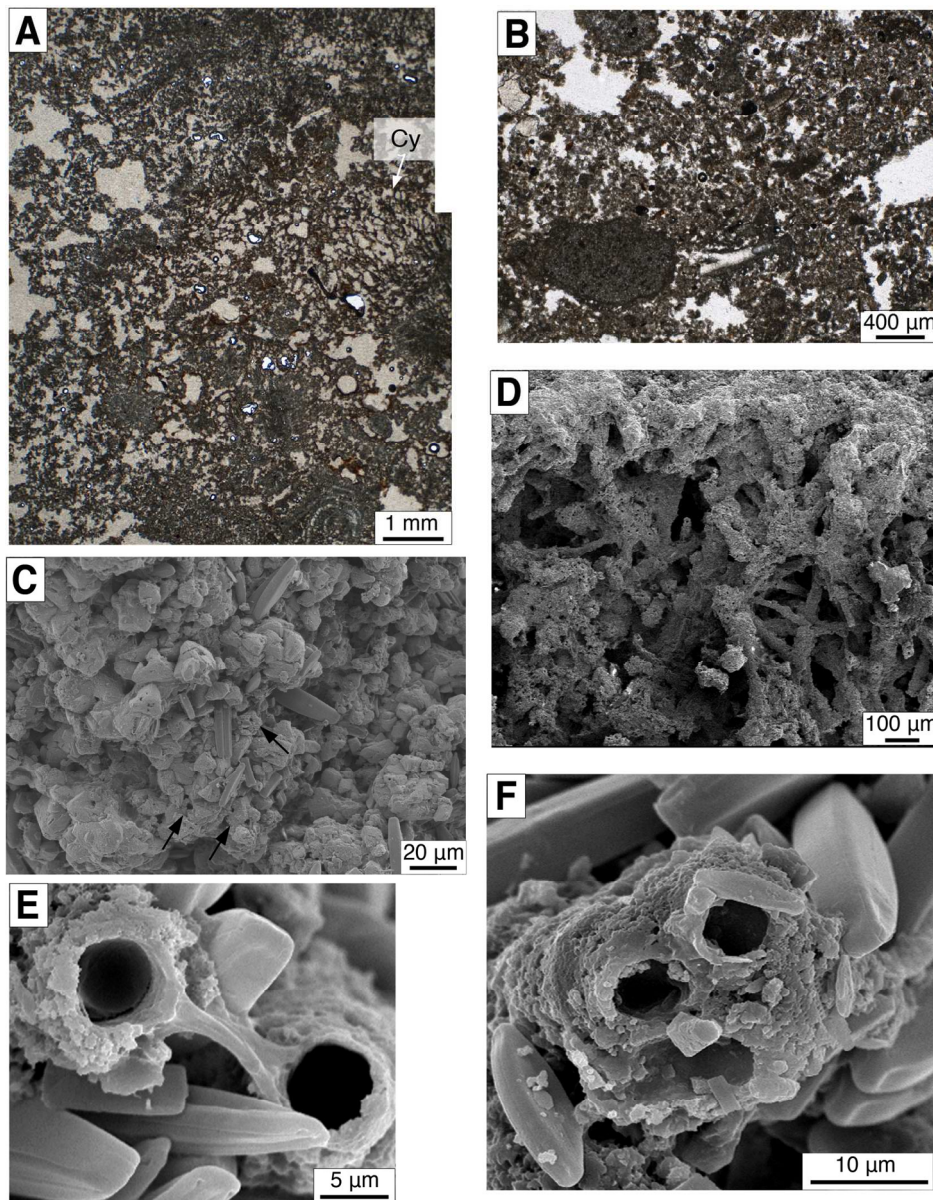


Fig. 4. Optical and scanning electron microscope images of samples selected from deposits formed on tablets installed in slow-flowing water areas (Facies B). (A) and (B) Typical loose, structureless sediment consisting of micrite with allochemical components (sections of calcite coated algae and macrophytes and intraclasts). Note in A the presence of a micrite mass evoking filamentous cyanobacteria (Cy). (C) Detail of texture of facies B: Isolated and clumped calcite crystals, diatoms and cyanobacterial tubes (arrowed). (D) Randomly oriented calcite tubes formed around cyanobacteria. Note that the inner diameter of most tubes is less than that of the tubes in Fig. C and D. (E) and (F) Calcite tubes (inner diameter = 5 μ m) consisting of small calcite crystals (1-2 μ m) and attached small diatoms. Note EPS in E and diatoms around the tubes.
169x216mm (250 x 250 DPI)

1
2
3
4
5
6
7
8
9
10
11
12
13
14
15
16
17
18
19
20
21
22
23
24
25
26
27
28
29
30
31
32
33
34
35
36
37
38
39
40
41
42
43
44
45
46
47
48
49
50
51
52
53
54
55
56
57
58
59
60

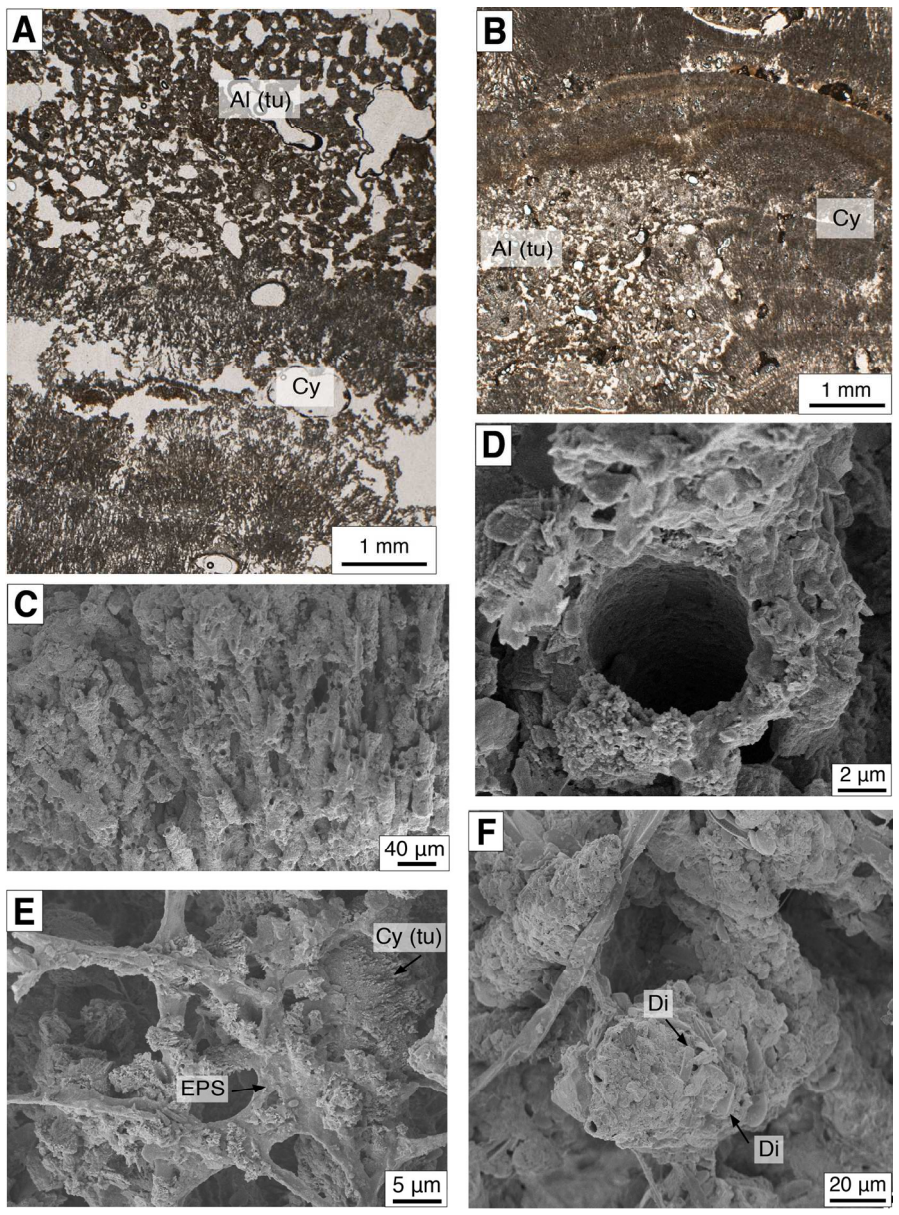


Fig. 5. Optical and scanning electron microscope images of samples selected from deposits formed on tablets installed in stepped waterfall areas (Facies C). (A) and (B) Association of stromatolites (laminae with tight filamentous cyanobacterial bodies) and boundstone consisting of coated filamentous algae (cross sections). (C) Mostly subvertical calcite tubes in stromatolite formed in a fast-flowing water zone. (D) Detail of calcite tube in C (inner diameter = 7 μ m). (E) Detail of calcite crystals associated with EPS and cyanobacterial tubes. (F) Randomly oriented calcite tubes (inner diameter = 2.5 μ m) consisting of thick calcite coatings containing attached diatoms. Note EPS around the tubes. Al (tu): Algae (tubes); Cy: Cyanobacteria; Cy (tu): Cyanobacteria (tubes); Di: Diatoms; EPS: Extracellular Polymeric Substances.
170x230mm (250 x 250 DPI)

1
2
3
4
5
6
7
8
9
10
11
12
13
14
15
16
17
18
19
20
21
22
23
24
25
26
27
28
29
30
31
32
33
34
35
36
37
38
39
40
41
42
43
44
45
46
47
48
49
50
51
52
53
54
55
56
57
58
59
60

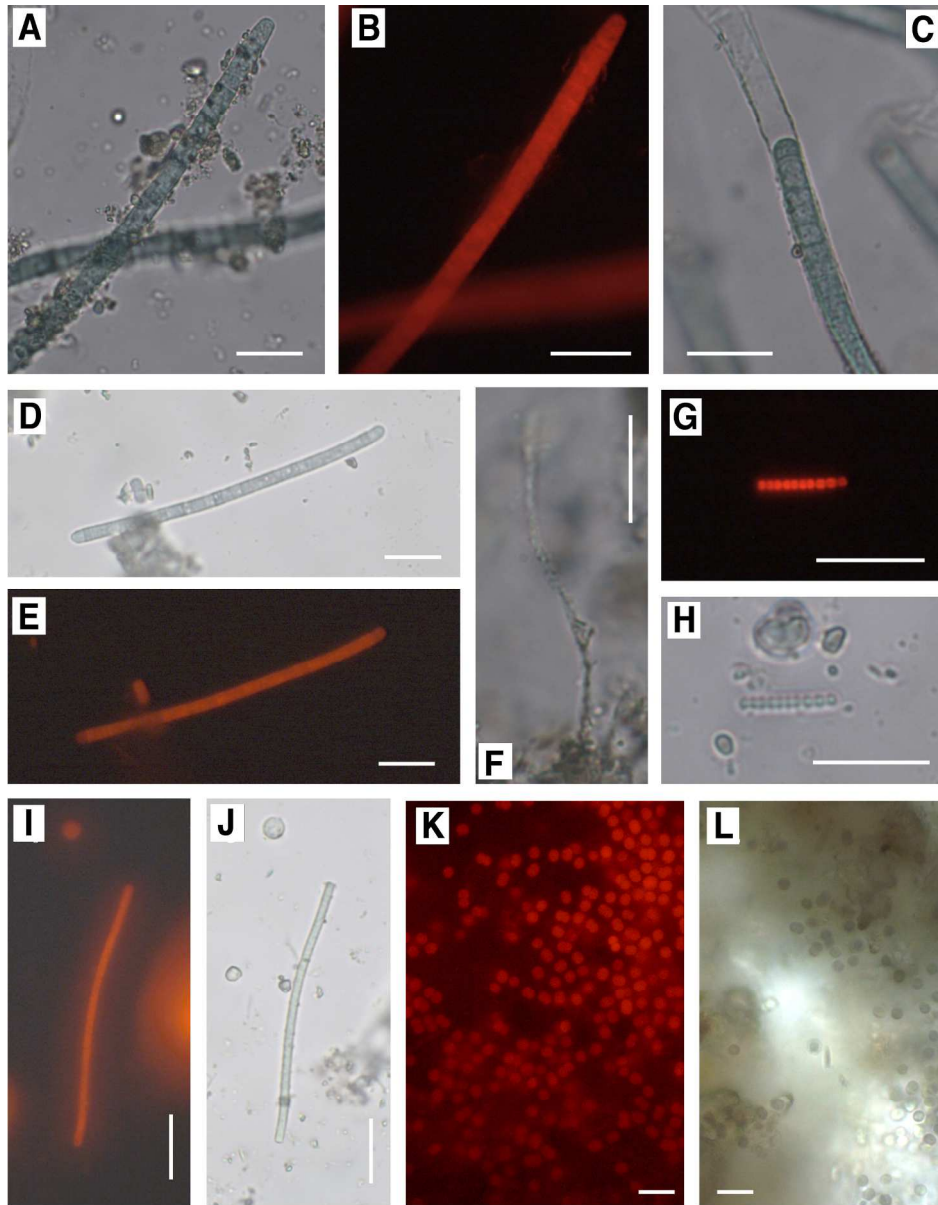


Fig. 6. Light and fluorescence microscopy photomicrographs showing the main cyanobacterial morphotypes identified in the samples. (A) and (B) *Phormidium incrustatum*; (C) *Phormidium aerugineo-caeruleum*; (D) and (E) *Phormidium* sp.; (F) *Leptolyngbya truncata*; (G) and (H) *Leptolyngbya foveolarum*; (I) and (J) *Leptolyngbya* sp.; (K) and (L) *Chamaesiphon* sp. Solid bars, 20 μ m.
187x239mm (299 x 299 DPI)

1
2
3
4
5
6
7
8
9
10
11
12
13
14
15
16
17
18
19
20
21
22
23
24
25
26
27
28
29
30
31
32
33
34
35
36
37
38
39
40
41
42
43
44
45
46
47
48
49
50
51
52
53
54
55
56
57
58
59
60

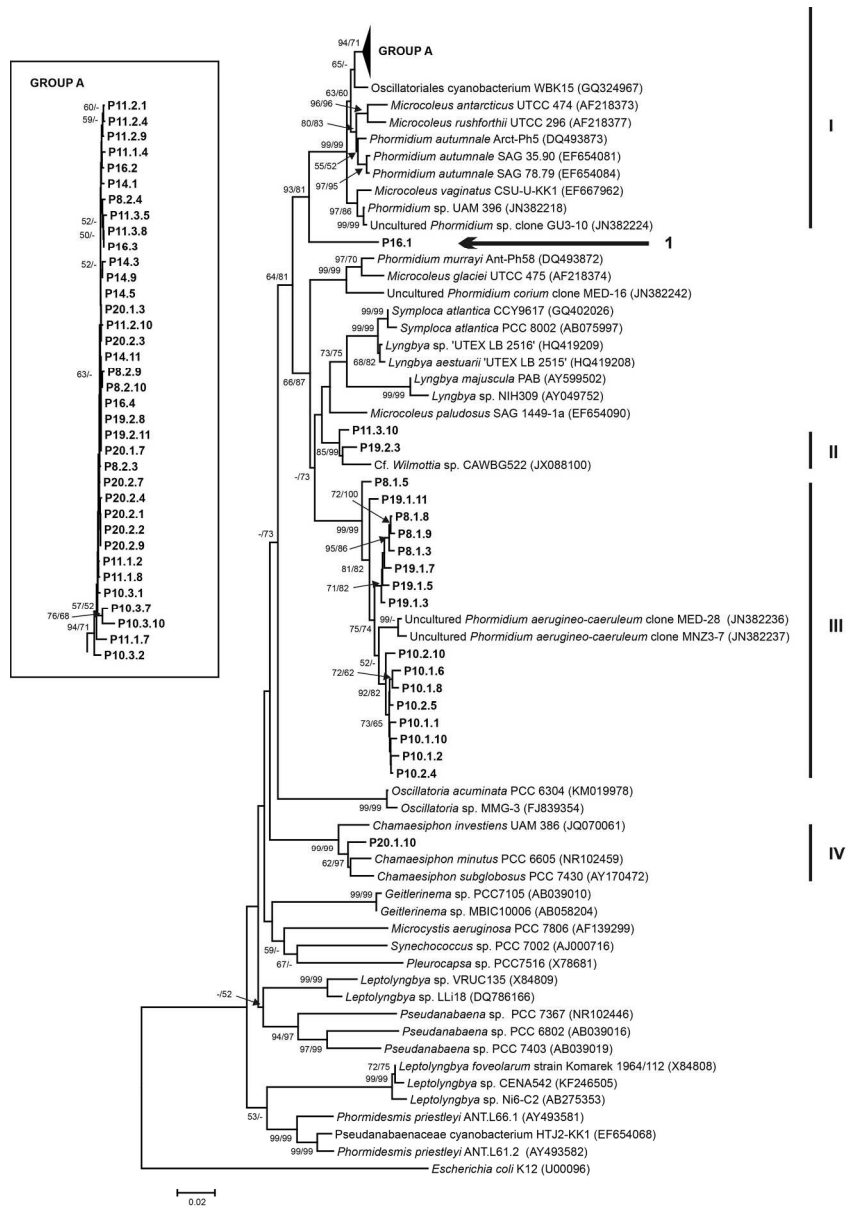


Fig. 7. Phylogenetic tree based on 16S rRNA gene sequences (1,315 positions) obtained by the neighbor-joining method. Bootstrap support from neighbor-joining and maximum likelihood analysis is reported above the nodes ($\geq 50\%$). Sequences from this study are indicated in bold and their associated GenBank accession numbers are listed in Table 4. GenBank accession numbers for database sequences are in parentheses following their name. The scale bar indicates 0.02 mutations per nucleotide position.
200x287mm (250 x 250 DPI)

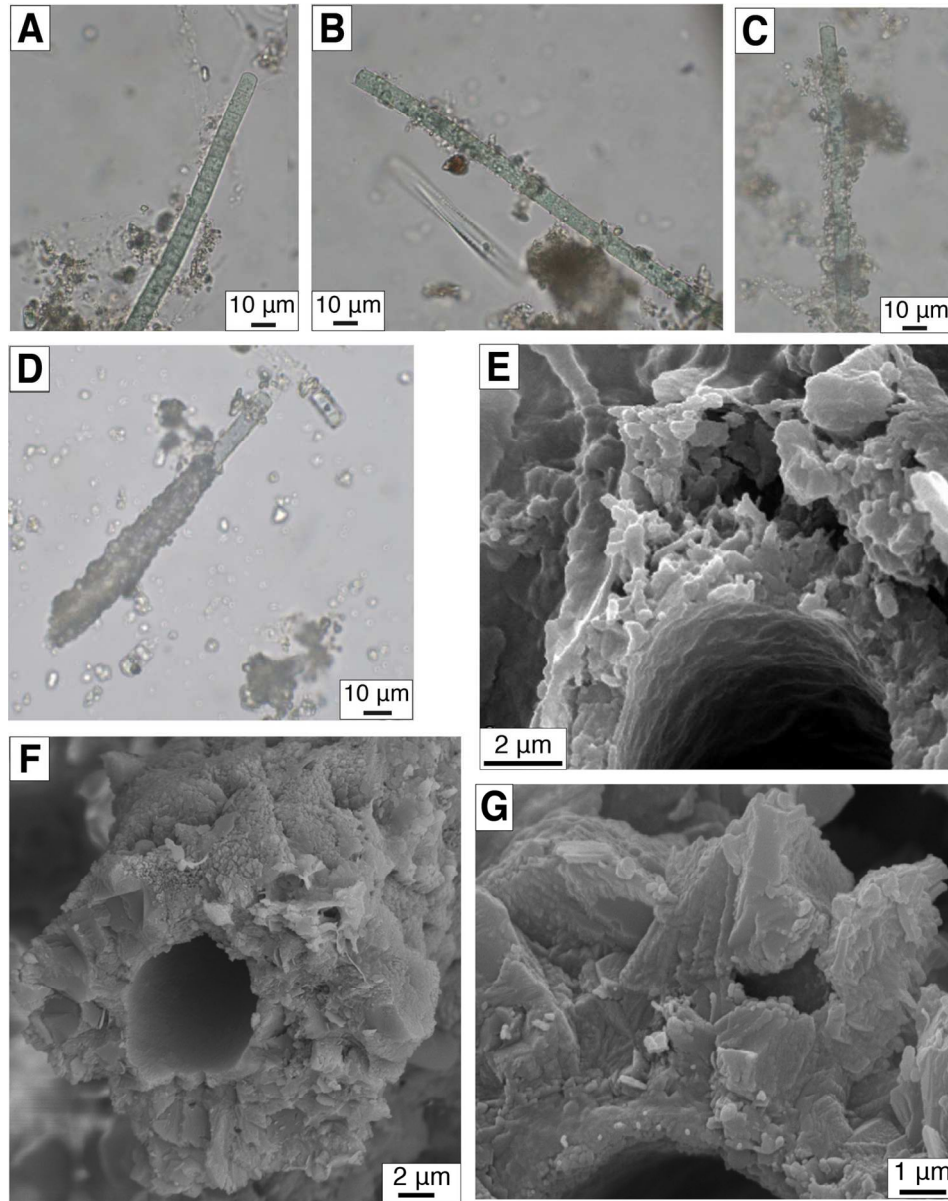


Fig. 8. (A) to (D) Optical microscope images of *Phormidium incrustatum* showing different degrees of calcification (samples taken on site from surface). Explanation in the text. (E) and (F) SEM images of CaCO_3 coatings formed around *Phormidium incrustatum* (samples from tablets). (E) Thin coating formed of irregular and small CaCO_3 forms. (F) and (G) Thick coatings showing larger crystals outwards. (H) and (I) SEM images of CaCO_3 coatings formed around *Phormidium aerugineo-caeruleum* (samples from tablets). Note the small and irregular CaCO_3 forms through the entire coating. (J) and (K) SEM images of CaCO_3 coatings formed around *Lyptolyngbya* (samples from tablets). Note the smaller size and irregular CaCO_3 forms in the interior and size increase of rhombohedra outwards.

167x211mm (250 x 250 DPI)

1
2
3
4
5
6
7
8
9
10
11
12
13
14
15
16
17
18
19
20
21
22
23
24
25
26
27
28
29
30
31
32
33
34
35
36
37
38
39
40
41
42
43
44
45
46
47
48
49
50
51
52
53
54
55
56
57
58
59
60

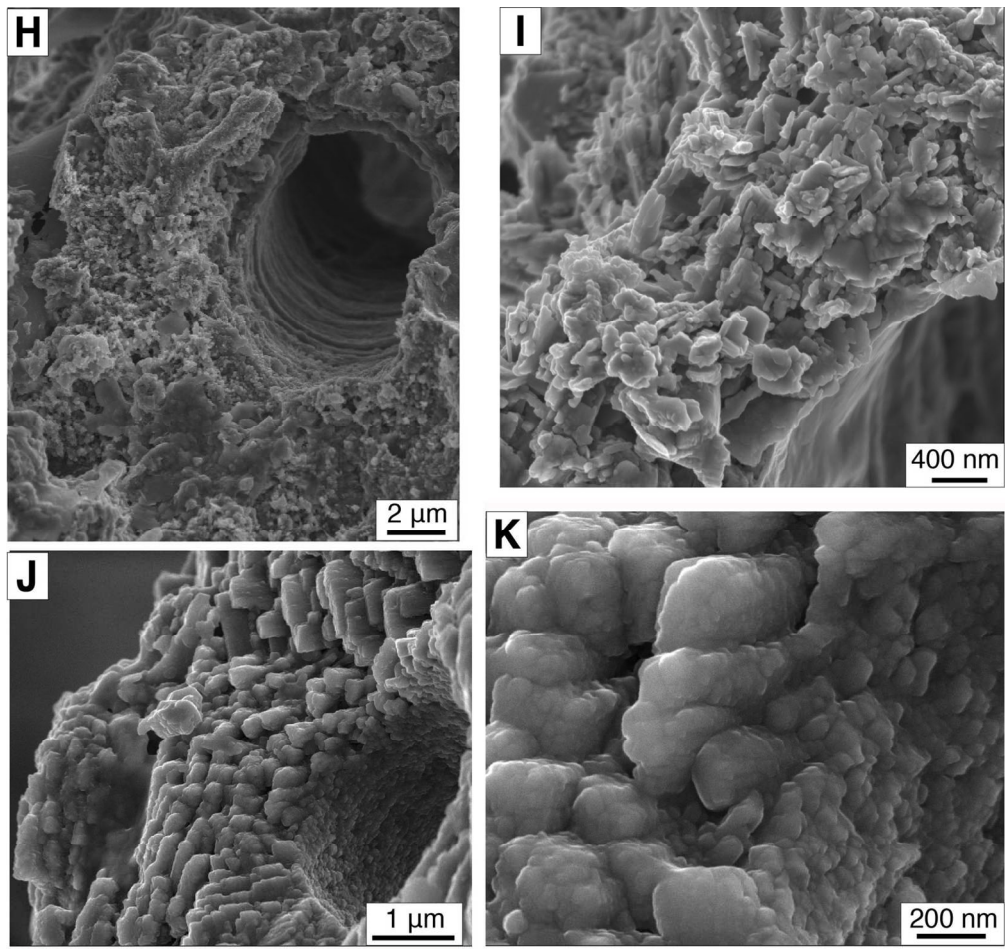


Fig. 8. (A) to (D) Optical microscope images of *Phormidium* *incrustatum* showing different degrees of calcification (samples taken on site from surface). Explanation in the text. (E) and (F) SEM images of CaCO_3 coatings formed around *Phormidium* *incrustatum* (samples from tablets). (E) Thin coating formed of irregular and small CaCO_3 forms. (F) and (G) Thick coatings showing larger crystals outwards. (H) and (I) SEM images of CaCO_3 coatings formed around *Phormidium* *aerugineo-caeruleum* (samples from tablets). Note the small and irregular CaCO_3 forms through the entire coating. (J) and (K) SEM images of CaCO_3 coatings formed around *Lyptolyngbya* (samples from tablets). Note the smaller size and irregular CaCO_3 forms in the interior and size increase of rhombohedra outwards.
168x158mm (250 x 250 DPI)

Table 1. Depositional environments, sedimentary facies and deposition rates of the sampled sites (Location of sites in Figure 1B).

Water velocity and depth correspond to maximum and minimum values measured at the end of the four seasons from 1999 to 2012. Deposition rates correspond to mean values from 1999 to 2012 for the sampled sites in this study. Warm periods: spring + summer seasons (6 months). Cool periods: autumn + winter seasons (6 months). Data compiled from Arenas et al. (2014).

Depositional environments Sampling sites	Water velocity (cm/s)	Water depth (cm)	Sedimentary facies	Mean deposition rates (mm)		
				Warm periods	Cool periods	Yearly
Areas of fast-flowing water, including steeper stretches along the riverbed, devoid of bryophytes and macrophytes. Sites P14, P16, P20.	90 – 260	7 – 11	A, Stromatolites: dense laminated deposits formed from cyanobacterial mats, preserved as tube-shaped calcite bodies subperpendicular to the substrate.	10.27	5.52	15.79
Areas of slow-flowing to standing water, upstream and downstream of waterfalls and barrages. Site 10-2.	20 - 80	10 – 45	B, Loose, commonly non-laminated deposits: Lime mud, varied mm-cm carbonate grains and macroscopic algae, with interbedded bacterial laminae. Rare oncoids. Boundstones of macrophytes in palustrine conditions.	0.76	1.92	2.68
Stepped waterfalls and small waterfalls (1 – 10 m high) with bryophytes and algae. Sites P8, P10-1, P11, P19.	30 -90	Water film (mm)	C, Mostly spongy tufa: mats of moss, macroscopic filamentous algae, cyanobacteria and herbaceous plants, coated by calcite. Rare and poor lamination and banding. In places, associated with facies A (e.g., P8 and P10-1).	5.97	3.03	9.00

Table 2: Tufa deposition and physical and chemical parameters of water at the sampled sites. Water temperature and velocity measured on site on 24 June and 23 September 2010 (between 10:00 and 12:00h). Hydrochemical parameters correspond to water samples collected on 24 June 2010 (conductivity and pH measured on site). Data compiled from Arenas et al. (2014). Location of sites in Figure 1B.

Sites	Facies	Tufa deposition (mm) April 2000 - Sept 2010	Water Temp (°C)		Water depth (cm)		Water velocity (cm/s)		Conduc-tivity (μS/cm)	Alkalin-ity (ppm HCO ₃)	Ca (ppm)	pH	log pCO ₂	Saturation index (calcite)
			June	Sept	June	Sept	June	Sept						
P8	C + A	3.5	15.5	16.3	9	11	132	43	619	276.2	95.2	8.2	-2.87	0.96
P10-2	B	5.1	15.7	16.4	24	21	42	28	660	267.4	82.4	8.1	-2.73	0.76
P11	C + A	4.8	15.6	16.3	0.5	0.5	89	70	640	260.8	79.5	8.1	-2.77	0.76
P14	A	9.6	15.6	16.4	10	9	259	253	644	261.0	79.6	8.4	-3.04	1.00
P16	A	10.4	15.7	16.5	7	5	172	181	512	261.3	81.5	8.4	-3.06	1.04
P19	C	2.7	16.1	16.7	0.5	0.5	-	-	503	244.2	78,0	8.2	-2.95	0.87
P20	A	10.7	16.0	16.8	8	7	205	203	514	253.2	80.2	8.4	-3.13	1.07

Table 3. Sampling sites, codes, accession numbers and closest relatives of sequences obtained from community DNA of cyanobacterial mats.

Sampling sites	Code	Accession numbers	Closest GenBank relative	Similarity %
P8	P8.2.3, P8.2.4, P8.2.9, P8.2.10	KP872586-89	<i>Phormidium autumnale</i> SAG 35.90	98
	P8.1.5	KP872583	<i>Phormidium aerugineo-caeruleum</i> mat MED clone 28	97
	P8.1.3, P8.1.8, P8.1.9	KP872582, 84-85	<i>Phormidium aerugineo-caeruleum</i> mat MED clone 28	98
P10-1	P10.3.1, P10.3.2, P10.3.7	KP872594, KP872635-36	<i>Oscillatoriales cyanobacterium</i> WBK15	99
	P10.3.10	KP872637	<i>Oscillatoriales cyanobacterium</i> WBK15	98
P10-2	P10.1.1, P10.1.2, P10.1.6, P10.1.8, P10.1.10, P10.2.4, P10.2.5, P10.2.10	KP872590-91, KP872631, KP872592, KP872632, KP872593, KP872633-34	<i>Phormidium aerugineo-caeruleum</i> mat MED clone 28	98
P11	P11.1.2, P11.1.4, P11.1.7, P11.1.8, P11.2.1, P11.2.4, P11.2.9, P11.2.10, P11.3.5, P11.3.8	KP872595-99, KP872600-04	<i>Phormidium autumnale</i> SAG 35.90	98
	P11.3.10	KP872605	Cf. <i>Wilmottia</i> sp. CAWBG522	98
P14	P14.1, P14.3, P14.5, P14.9, P14.11	KP872606-10	<i>Phormidium autumnale</i> SAG 35.90	98
P16	P16.1	KP872611	<i>Phormidium autumnale</i> Arct-Ph5	93
	P16.2, P16.3, P16.4	KP872612-14	<i>Phormidium autumnale</i> SAG 35.90	98
P19	P19.2.8, P19.2.11	KP872620-21	<i>Phormidium autumnale</i> SAG 35.90	98
	P19.2.3	KP872619	Cf. <i>Wilmottia</i> sp. CAWBG522	98
	P19.1.11	KP872618	<i>Phormidium aerugineo-caeruleum</i> mat MED clone 28	97
	P19.1.3 P19.1.5, P19.1.7	KP872615-17	<i>Phormidium aerugineo-caeruleum</i> mat MED clone 28	98
P20	P20.1.10	KP872624	<i>Chamaesiphon subglobosus</i> PCC 7430	98
	P20.1.3, P20.1.7, P20.2.1, P20.2.2, P20.2.3, P20.2.4, P20.2.7, P20.2.9	KP872622-23, KP872625-30	<i>Phormidium autumnale</i> SAG 35.90	98

Table 4. Relative abundance (%) of cyanobacteria (with respect to total cyanobacteria) determined from optical microscope examination at each sampled site in this study. Location of sites in Figure 1B.

Species	Sites							
	P8	P10-1	P10-2	P11	P14	P16	P19	P20
<i>P. incrustatum</i>	87	78	10	33	75	77	72	98
<i>P. aerugineo-caeruleum</i>	5	13.5	75	55	0	0	16.5	0
<i>Phormidium</i> sp.	0	1.5	5	5	18.5	16	4.3	0
<i>Leptolyngbya foveolarum</i>	4	1.5	3.5	1.5	1	0	1	0
<i>Leptolyngbya truncata</i>	1	0	0	<1	0	2	1	0
<i>Leptolyngbya</i> sp.	<1	1	0	<1	1	1.5	2	0
<i>Aphanocapsa</i> sp.	1.4	1.5	3	<1	1.5	1.5	1.2	0
<i>Aphanothece</i> sp.	1	2	3	2	3	2	2	0
<i>Chamaesiphon</i> sp.	0	<1	<1	1	0	0	0	2

Table 5. Comparison of sedimentary facies, deposition rates, morphotypes and phylotypes at each sampled site. Deposition rates from thickness measurements on tablets from Arenas et al. (2014).

Location of sites in Figure 1B.

Sites	Sedimentary facies	Deposition (mm) April 2000-Sept 2000	Mean yearly deposition (mm) April 1999-Sept 2012	Dominant morphotype	Phylotypes
P8	C + A	3.52	7.88	<i>P. incrustatum</i>	I, III
P10-1	C + A	4.17	9.33	<i>P. incrustatum</i>	I
P10-2	B	5.13	2.68	<i>P. aerugineo-caeruleum</i>	II, III
P11	C + A	4.85	10.29	<i>P. incrustatum</i> <i>P. aerugineo-caeruleum</i>	I, II
P14	A	9.58	16.02	<i>P. incrustatum</i>	I
P16	A	10.38	16.53	<i>P. incrustatum</i>	I, V
P19	C	2.74	7.99	<i>P. incrustatum</i>	I, II, III
P20	A	10.70	14.80	<i>P. incrustatum</i> <i>Chamaesiphon sp.</i>	I, IV